Chemical Engineering Journal 481 (2024) 148417

Contents lists available at ScienceDirect

Chemical Engineering Journal

journal homepage: www.elsevier.com/locate/cej

Hydrogel-assisted microfluidic wet spinning of poly(lactic acid) fibers from a green and pro-crystallization spinning dope

Wuchao Wang [a], Jonathan Avaro [a,b], Tobias Hammer [a], Lucyna Hämmerle [a,c], Bruno F. B. Silva [a,b,c], Luciano F. Boesel [a], René M. Rossi [a,*], Kongchang Wei [a,c,*]

[a] Empa, Swiss Federal Laboratories for Materials Science and Technology, Laboratory for Biomimetic Membranes and Textiles, Lerchenfeldstrasse 5, 9014 St. Gallen, Switzerland
[b] Empa, Swiss Federal Laboratories for Materials Science and Technology, Center For X-Ray Analytics, Lerchenfeldstrasse 5, 9014 St. Gallen, Switzerland
[c] Empa, Swiss Federal Laboratories for Materials Science and Technology, Laboratory for Biointerfaces, Lerchenfeldstrasse 5, 9014 St. Gallen, Switzerland

ARTICLE INFO

Keywords:
Microfluidic wet spinning
Green solvent
PLA fibers
Hydrogel
Medical textile

ABSTRACT

Poly(lactic acid) (PLA) fibers have found a broad range of applications in medical textiles. While traditional spinning methods usually involve harsh conditions, such as high temperature or toxic organic solvents, the challenges in producing PLA fibers via a green route are yet to be overcome. Herein, we described a new strategy for PLA fiber production, which combines the controlled and benign spinning conditions enabled by microfluidics and a novel green spinning dope with bio-sourced Cyrene™ as a non-toxic solvent for PLA. This strategy is enabled by the in-situ formation of a hydrogel shell around the focused PLA/Cyrene™ spinning dope stream. This hydrogel shell stabilizes the core stream and facilitates the solidification of the PLA fiber. Our hydrogel-assisted microfluidic wet spinning (HA-MWS) strategy represents the first-ever method that allows for the continuous room-temperature production of highly porous PLA fibers (porosity > 80 %) without the need for petroleum-based chemicals. We characterized the solution properties of the PLA/Cyrene™ spinning dope and discovered that Cyrene™ can induce PLA crystallization, with resultant crystals acting as cross-linking centers for the spinning dope gelation. We then explored the microfluidic wet spinning process, using the spinning dope as the core flow and the alginate aqueous solution as the shell flow to achieve controlled fiber production. The resulting PLA fibers underwent comprehensive morphological, structural, and mechanical characterization. Our process enables the green production of PLA fibers under mild conditions. More importantly, a bio-based green and pro-crystallization solvent was for the first time used to develop PLA spinning dope, which gives rise to a range of promising fiber properties (e.g. high porosity), which can broaden potential biomedical applications of PLA fibers.

1. Introduction

Poly(lactic acid) (PLA) is an aliphatic bio-based polyester derived from renewable resources like corn and sugarcane. As a promising sustainable alternative for petroleum-based polymers [1], its production accounts for 18.7 % of the total global production of bio-plastics as of 2020 [2]. Owing to the excellent biocompatibility of the polymer and the degradation product (i.e., lactic acid), PLA has been extensively used in various medical applications [3]. In particular, PLA fibers are important building blocks of various medical devices [4]. For instance, PLA fibers have been used in commercial surgical sutures and blood vessel stents [5]. A recent clinical implantation of PLA fiber-based occluder has demonstrated its potential for closure of atrial septal defect in cardiovascular disease (CVD) patients [6]. PLA fiber materials have also found promising applications in bone tissue engineering [7], peripheral nerve repair [8], urinary bladder reconstruction [9], drug delivery and sustained release [10], as well as bacterial infection prevention [11].

Commercial PLA fibers for the abovementioned medical applications are generally produced by melt spinning at high processing temperatures (185–240 °C) [12–14]. While the high spinning temperatures can lead to thermal and hydrolytic degradation, solution-based wet spinning

* Corresponding authors at: Empa, Swiss Federal Laboratories for Materials Science and Technology, Laboratory for Biomimetic Membranes and Textiles, Lerchenfeldstrasse 5, 9014 St. Gallen, Switzerland.
E-mail addresses: rene.rossi@empa.ch (R.M. Rossi), kongchang.wei@empa.ch (K. Wei).

https://doi.org/10.1016/j.cej.2023.148417
Received 8 October 2023; Received in revised form 13 December 2023; Accepted 27 December 2023
Available online 2 January 2024

can produce PLA fibers under mild condition, usually at room temperature with PLA non-solvents as coagulants [15]. This makes it particularly attractive for loading and delivery of bioactive cargos in PLA fibers for biomedical applications [16–18]. Currently, the preparation of PLA spinning dopes heavily relies on petroleum-based organic solvents. Some PLA solvents are known as ε solvents, which can induce PLA solution crystallization (ε form PLA-solvent complex) and subsequent gelation. Such ε solvents include dimethylformamide (DMF), cyclopentanone (CPO), 1,3-dioxolane (DOL), γ-butyrolactone (GBL), and tetrahydrofuran (THF) [19]. However, non-ε solvents such as dichloromethane (DCM) [16], methylene chloroform [20], chloroform [21], dimethyl sulfoxide (DMSO) [22], N-methyl pyrrolidone (NMP) [22], and hexafluoroisopropanol (HFIP) [23] were mainly used for wet spinning of PLA fibers. In recent years, to reduce the environmental impact of PLA fiber production, a few "greener" solvent systems have been proposed for dissolving PLA polymers, including binary systems such as ethyl acetate/DMF [24] and ethyl acetate/DMSO [25], as well as single-solvent systems such as ethyl lactate [26] and dimethyl carbonate [27]. Nevertheless, these "greener solvents" for PLA fiber spinning still rely much on fossil resource [28]. A fully bio-based PLA spinning system for sustainable and green fiber production is yet to be developed.

As an emerging wet spinning technology, microfluidic wet spinning (MWS) confines coaxial laminar flow within a micrometer-scale channel, where the fiber formation can be induced by various methods, including solvent exchange, ionic crosslinking, and photopolymerization [29,30]. In addition to the flexibility in choosing controlled fiber solidification methods, the precise tuning of flow conditions enabled by nowadays commercial microfluidic pumping systems offers delicate manipulation of liquid flow conditions, which allows the control over fiber structural and mechanical properties by microfluidic wet spinning [31,32]. This feature makes MWS particularly attractive for the production of bio-based polymer fibers (Supporting information, Table 1). For instance, Zhang X. and co-workers reported the production of alginate polymer fibers via MWS, demonstrating that, not only the fiber diameter, but also the macromolecule orientation within fibers can be tuned by varying the spinning parameters, which showed a significant impact on the tensile strength of resultant fibers [33,34]. Nie S. and co-workers demonstrated the capability of MWS in flow-controlled twisting of cellulose nanocrystal (CNC) orientation during the fiber forming process, which led to the improved mechanical properties [35]. In a recent attempt, PLA fibers were also successfully produced via MWS with DCM as solvent. Nevertheless, like traditional wet spinning, MWS of PLA fibers with bio-based solvents is yet to be achieved.

With the development of green chemistry, various new solvents have been developed from renewable feedstocks. Such new solvents include oils/citrus waste-based green solvents such as Cymene® and Limonene®, lignocellulosic based green solvents such as γ-Valerolactone (GVL), and cellulose derived solvents such as tetrahydrofurfuryl-alcohol (THFA) and Cyrene™ [36]. Cyrene™, in particular, is extracted from cellulose in two steps. It is considered a biodegradable, non-toxic and renewable solvent, with high boiling temperature (227 °C) and similar polarity (0.91, π^a) to traditional polar solvents such as DMF, DMAc, NMP [37,38]. According to the hierarchical solvent selection guide for medical chemists, Cyrene™ is a valuable option for medical applications because of its better performance in safety and health protection [39]. It has been used to dissolve various polymers, including polyvinylidene fluoride (PVDF), polylactic-co-glycolic acid (PLGA), polyethersulfone (PES), polyhydroxyalkanoate (PHA) and polyvinylpyrrolidone (PVP), among others [40–44]. However, Cyrene™ has a low miscibility with water (52.6 g Cyrene™ /L water), and a high water-Cyrene™ interfacial tension (72.5 mN·m^{-1} at 25 °C) [45]. This makes it challenging to establish stable laminar flows of polymer/Cyrene™ solutions within water-based shell flow. In addition, its high viscosity (14.6 cP) also makes it difficult to be removed from the resulting polymeric products [45]. Consequently, the potential of Cyrene™ in polymer fiber spinning is not yet realized.

In this study, the potential of Cyrene™ as a green solvent for MWS of PLA fibers was explored. Firstly, the time-dependent PLA/Cyrene™ solution properties were characterized. Reversible "sol-gel" transition was discovered. Detail investigation revealed that the gelation was induced by PLA crystallization. The pro-crystallization property of Cyrene™ for PLA was not known from abovementioned non ε-solvents used for PLA fiber spinning, and herein investigated in detail. Subsequently, to overcome the abovementioned challenges and explore the potential of bio-based MWS of PLA fibers, we herein developed a hydrogel-assisted MWS (HA-MWS) method, leading to successful production of PLA fibers with a PLA/Cyrene™ solution as the spinning dope. More specifically, the HA-MWS strategy involves solidifying PLA fibers by water-Cyrene™ exchange, which took place within the temporally in-situ formed alginate (Alg)-Ca^{2+} hydrogel shell. This is enabled by the PLA-Alg core–shell flows established in a coaxial microfluidic device. After spinning, the Alg-Ca^{2+} hydrogel shell allows long-term solvent exchange between the PLA/Cyrene™ core and the surrounding aqueous environment, thus assisting the complete solidification of PLA fibers and removal of Cyrene™ solvent. With this green production excluding any usage of petroleum-based toxic solvents, highly porous PLA fibers (porosity above 80 %) were achieved after removing the Alg-Ca^{2+} hydrogel shell in a sodium chloride aqueous solution.

To the best of our knowledge, no bio-based ε solvent has been reported for PLA before. PLA-solvent crystal complex were only reported in a few petroleum-based ε solvents, *i.e*·THF, CPO, DOL, GBL and DMF. Among these ε solvents, only DMF can induce the formation of PLA/solvent cocrystal and gel at room temperature, others require much lower temperatures [19]. This is the first report of bio-based green solvent (Cyrene™) for inducing PLA crystallization and "sol-gel" transition at room temperature. By using such a fully bio-based and pro-crystallization spinning dope, highly porous PLA fibers were spun at room temperature for the first time with a green method excluding any usage of petroleum-based organic solvents.

2. Experimental Section

2.1. Materials

Poly(lactic acid) (PLA) (Ingeo3100 HP NatureWorks LLC, *Mw* = 148,250 g/mol) was purchased from NatureWorks LLC. Sodium alginate (W201502), calcium chloride ($CaCl_2$), sodium chloride (NaCl), Cyrene™, N,N-Dimethylformamide (DMF, ≥99.8 %), Dulbecco's Modified Eagle Medium (DMEM, Lot. D5796), fetal bovine serum (FBS, Lot. F9665), and 1 % penicillin/streptomycin (P/S, Lot. P4458), human recombinant basic fibroblast growth factor (bFGF, Lot. 01–106) were purchased from Sigma Aldrich, and used as received. Human dermal fibroblasts were purchased from CELLnTEC (HDF, Lot. EB1104281, juvenile donor). CellTiter 96® Non-Radioactive Cell Proliferation Assay kit (MTT, Lot. G4000) was purchased from Promega.

2.2. Calculation of Hildebrand solubility parameter and relative energy difference between Cyrene™ and PLA

Hildebrand solubility parameter (δ_t) was calculated according to Equation (1), and used for predicting polymer solubility in different solvents [46].

$$\delta_t = \sqrt{{\delta_d}^2 + {\delta_p}^2 + {\delta_h}^2} \quad (1)$$

Where δ_d is dispersion force, δ_p is intermolecular interaction and δ_h is hydrogen bonding interaction. The difference value ($\Delta\delta$) between polymer (δ_{tp}) and solvent (δ_{ts}) determines whether the solvent is a benign solvent ($\Delta\delta < 2$) or poor solvent ($\Delta\delta > 2$) for the given polymer, as described for Equation (2).

$$\Delta\delta = |\delta_{tp} - \delta_{ts}| \quad (2)$$

In addition, solvent modified radius (R_a) was calculated according to Equation (3),

$$R_a = \sqrt{4(\delta_{dp} - \delta_{ds})^2 + (\delta_{pp} - \delta_{ps})^2 + (\delta_{hp} - \delta_{hs})^2} \quad (3)$$

Where, δ_d is dispersion force, δ_p is intermolecular interaction and δ_h is hydrogen bonding interaction, and the subscript with p and s stands for corresponding value of polymer and solvent. R_a is solvent modified radius, R_0 is polymer modified radius (R_0 for PLA is 10.5). Relative energy difference (RED) is the ratio between R_a and R_0 (Equa. 4), indicating benign (RED < 1) or poor solvent (RED > 1) [47].

$$RED = R_a/R_0 \quad (4)$$

2.3. Preparation of PLA/Cyrene™ and PLA/DMF solution as spinning dope

Based on the high boiling temperature of solvents (Cyrene™ and DMF) and thermoplastic property of PLA, high heating temperature was chosen to dissolve PLA. 10 g of PLA were dissolved in Cyrene ™ or DMF at 120 °C for 3 h under vigorous stirring, giving rise to a clear yellowish or white PLA solution (10 wt%) after complete polymer dissolution, respectively. The freshly prepared solution was either used as spinning dope after cooling down to room temperature (in a circulating water bath for ~ 10 min), or stored at 4 °C for later application. Stored solutions were re-heated to 120 °C for 30 min before use as spinning dope at room temperature.

2.4. Rheological characterization of PLA/Cyrene™ and PLA/DMF solution property

After the PLA was completely dissolved and freshly cooled down to room temperature, the PLA/Cyrene™ and PLA/DMF solution rheological properties were investigated with a stress-controlled rheometer (MCR 301, Anton Paar). Steady state viscosity measurements were done at room temperature with a cone plate (0.996 degree, 50 mm in diameter). Long-term stability was characterized by oscillatory time-sweep (1 % strain, 1 Hz) with the same cone plate setup at room temperature.

2.5. FT-IR characterization of PLA/Cyrene™ solution property

Attenuated total reflectance Fourier-transform infrared spectroscopy (AT-FTIR, 640-IR, Agilent Technologies) was used to characterize the time-dependent PLA/Cyrene™ solution property by monitoring the inter- and intra-molecular interactions (from 500 to 4000 cm^{-1} with a spectral resolution of 1 cm^{-1}).

2.6. X-ray diffraction (XRD) analysis

The D8 Advance diffractometer (Bruker company) with Apex II CCD-Detector and equipped with a Cu Kα X-ray tube operated at 40 kV and 40 mA was used to characterize the crystal structure of PLA gels. After 10 wt% PLA/Cyrene™ was re-heated to 120 °C and cooled down to room temperature, PLA solution was added to test platform and then scanned in different times when it was kept in the platform. The crystal structure of PLA fibers was characterized by a powder X-ray Diffractometer (Empyrean 3, Malvern Panalytical), which is equipped with a Cu Kα X-ray source (operated at 40 kV and 20 mA), a PIXcel 1D detector, and a scintillation counter.

2.7. Polarized optical microscopy (POM) analysis

The POM (AxioImager.Z2, Zeiss) equipped with two polarization filters (polarization orientation rotation 360°, each for excitation and detection light path once). A thin layer of PLA/Cyrene™ gel was loaded on a microscopy glass slide and compressed by another glass slide for flattening the sample.

2.8. Fabrication of PDMS-based microfluidic chip

The Polydimethylsiloxane (PDMS)-based microfluidic chip, as shown in Supporting Information, **Fig. S1**, was fabricated with a molding method adapted from our previous work [48]. Briefly, 21 G and 18 G stainless steel needles (Sterican, VWR) were assembled in a core–shell aligned structure supported by Lego® blocks. Such a Lego®-needle hybrid mold was placed in a glass dish. In the meantime, the PDMS prepolymer was mixed with crosslinker (Sylgard® 184, Dow Corning) in a weight ratio of 10:1, and the complete mixture of PDMS precursor was then de-bubbled under vacuum for at least 1 h. Then the prepared precursor was poured into the abovementioned glass dish to cover the hybrid mold. After curing at 80 °C for 2 h in an oven, the molded PDMS elastomer was cooled down to room temperature, before needles and Lego® blocks were removed from the PDMS elastomer. With ethanol as lubricant, glass capillaries were then inserted into corresponding channels (inlet channel capillary: OD 1.02 mm ID 0.72 mm, outlet: OD 1.86 mm ID 1.32 mm).

2.9. Green HA-MWS spinning strategy

While PLA is a product from renewable resources like corn and sugarcane, supplementary polymers and solvents from bio-based resources were chosen to enable green production of PLA fibers via microfluidic wet spinning (Fig. 1). Specifically, Cyrene™ (cellulose-derived solvent) was used to dissolve PLA for preparing the spinning dope. Subsequently, PLA/Cyrene™ solution (as the core flow in a co-axial microfluidic chip) will be hydrodynamically shaped by alginate (from seaweed) aqueous solution as shell flow (Fig. 1**A-C**). With such a fully bio-based material system, PLA fibers were spun by a hydrogel-assisted microfluidic wet spinning (HA-MWS) method (Fig. 1**C**), where the alginate shell flow formed hydrogel layers immediately in the $CaCl_2$ collection bath due to the rapid gelation induced by Alg-Ca^{2+} cross-linking. The solidifying PLA core flow was trapped within the alginate hydrogel shell formed in-situ (Fig. 1**C**). Thereafter, the PLA fibers were homogeneously solidified under hydrogel shell protection and Cyrene™-water solvent exchange (Fig. 1**D**). After the solvent exchange was complete, the Alg-Ca^{2+} hydrogel shell was removed by simply soaking the fibers in NaCl aqueous solution (Fig. 1**E**), giving rise to final PLA fibers (Fig. 1**F**).

2.10. PLA fiber spinning and post-spinning treatments

PLA fibers were spun at room temperature, with liquid flow rates controlled by neMESYS 290 N Cetoni® pumps. In a typical process, PLA solution was flowed into the core channel at different flow rates, and alginate aqueous solution, i.e. Alg (aq) with different concentrations (2 wt%, 4 wt%, and 5 wt%) were introduced from the side inlet as shell flow, giving rise the core–shell co-axil laminar flow at the hydrodynamic focusing position. The established PLA-Alg core–shell flow was injected into a collection bath containing 0.7 wt% $CaCl_2$ solution, where the as-spun PLA-Alg fibers were collected.

The as-spun PLA-Alg fibers collected in the 0.7 wt% $CaCl_2$ bath at room temperature were transferred to and kept in a bath of DI water (200 mL), to allow further solvent exchange between Cyrene™ and water for an additional 4 days. The PLA-Alg core–shell fibers were then immersed into 25 wt% NaCl aqueous solution to remove Alg-Ca^{2+} hydrogel shell layer. To completely remove the hydrogel shell, the PLA-Alg fibers were immersed in NaCl aqueous solution for 1 h. After that, the NaCl (aq) was refreshed 2 times (10 min for each period) with manual stirring of a glass stirring rod, before the resultant PLA fibers were rigorously washed by DI water (4 times, 10 min for each period) to

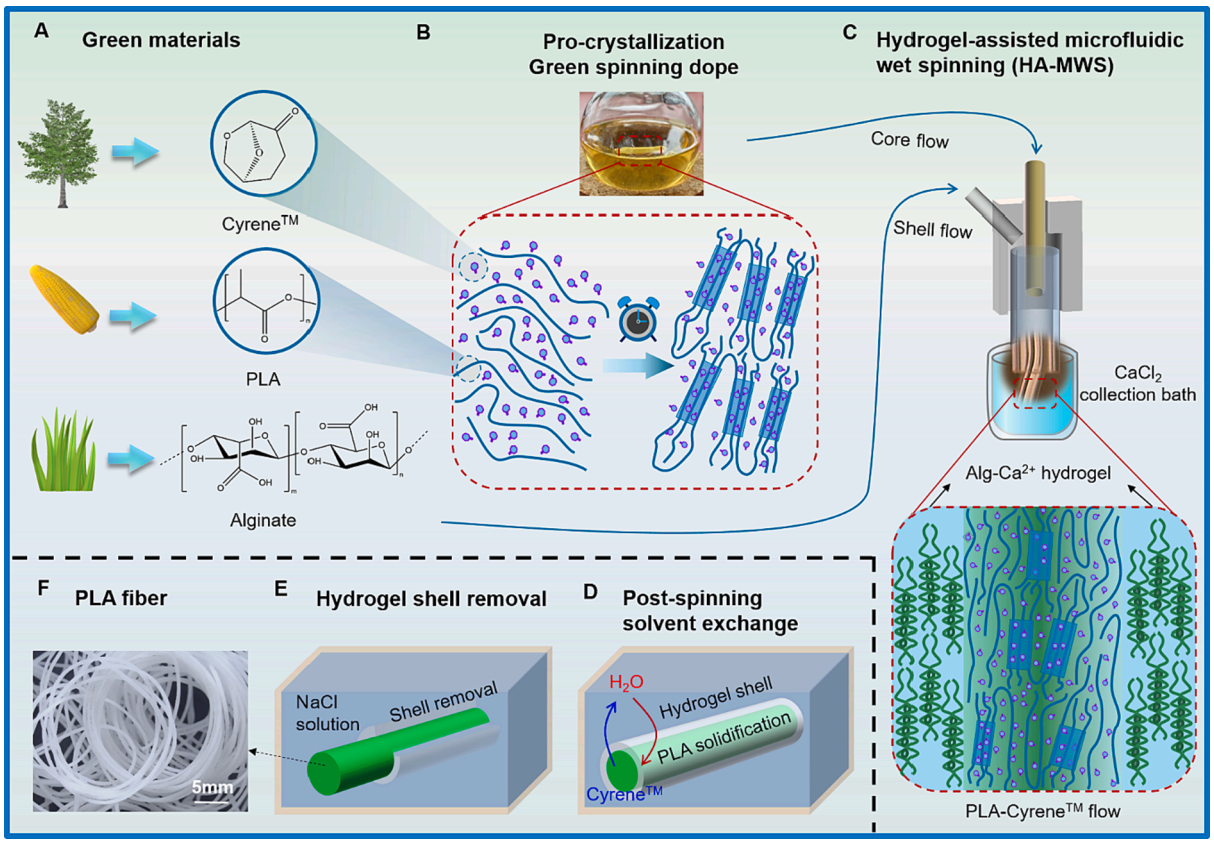

Fig. 1. Hydrogel-assisted microfluidic wet spinning (HA-MWS) of PLA fibers. **(A)** Bio-based materials for PLA fiber spinning. **(B)** PLA/Cyrene™ spinning dope containing PLA-solvent cocrystals. **(C)** Solidifying PLA core in the in-situ formed Alg-Ca^{2+} hydrogel shell. **(D)** Post-spinning solvent exchange for further solidification of PLA fibers. **(E)** Removal of the Alg-Ca^{2+} hydrogel shell by soaking in NaCl aqueous solution. **(F)** A representative digital photo of the resultant PLA fibers.

remove NaCl. The PLA fibers were then dried in a vacuum oven at 40 °C for 2 h.

2.11. Characterization of solvent exchange

To monitor the process of solvent exchange, the as-spun PLA-Alg fibers were placed in a 200 mL bath of DI water at room temperature. The diffusion of Cyrene™ into the water bath was monitored with UV–Vis absorbance of Cyrene™. Briefly, a 2 mL water sample was taken from the bath after different solvent exchange period (4 h, 24 h, 48 h, 72 h and 96 h, respectively) for UV–Vis measurement, followed by the complete renewal of DI water in the bath. Ultraviolet–visible (UV–Vis) absorption spectrum was taken for all the samples for analyzing the Cyrene™ content by using a UV–Vis spectroscopy (Cary 4000, Ailgent).

2.12. Thermogravimetric analysis (TGA)

After each sample was dried in the oven for 4 h at 40 °C, PLA fibers were tested by thermogravimetric analysis with a thermogravimetric analyzer (TG 209 F1 Libra, Netzsch). These fiber samples were weighed (mass below 5.0 mg), placed into ceramic crucibles, and heated accordingly. All tests were conducted under a nitrogen flow (250 mL/min) with heating range from 50 °C to 800 °C at a constant heating rate of 10 °C/min.

2.13. Differential scanning calorimetry (DSC) characterization

Differential scanning calorimetry (DSC, 214 Polyma, Netzsch) was used to characterize the crystallinity of spinning dope and PLA fibers. Spinning dope was refreshed at 120 °C for 30mins and quickly flushed with tap water around the flask for 10 min to cool it down to room temperature. 5 PLA/Cyrene™ samples and 1 PLA/DMF sample of spinning dope with 4–20 mg were prepared for DSC characterizations. Spinning dope and fiber samples were tested from 25 °C to 250 °C in nitrogen atmosphere at a heating rate of 10 °C/min. The software on NETZSCH Proteus Thermal Analysis 8.0.2 was used to measure melting enthalpy. The calculation on enthalpy of spinning dope by the software set the temperature of onset (55 °C) and end-point (65 °C). For the fiber, the onset and end-point for calculating the area of peak in melting enthalpy were set at 165 °C and 185 °C, respectively.

The degree of crystallinity (X_C) was calculated according to Equation (5) (Equa. 5):

$$X_C = \frac{\Delta Hm}{\Delta Hmp} \times 100\% \quad (5)$$

where ΔHm is the melting enthalpy of the tested samples, and ΔHmp (93.6 J/g) is the reference melting enthalpy of 100 % crystalline PLA [49].

2.14. Wide-Angle X-ray scattering (WAXS) measurements

Wide-Angle X-ray Scattering (WAXS) measurements were carried out using a Bruker Nanostar instrument (Bruker AXS GmbH, Karlsruhe, Germany). This instrument is equipped with a micro-focused X-ray Cu source (wavelength Cu Kα = 1.5406 Å) and a pinhole-collimation system, providing a beam size of ca. 400 μm at the sample position. A custom-built semitransparent beamstop was used in the setup, along with a VÅNTEC-2000 detector with a resolution of 2048 × 2048 pixels, each with a size of 68 × 68 μm^2. The WAXS measurements were performed at a sample-to-detector distance (SDD) of 5 cm. The SDD was precisely determined using corundum as a calibrant, providing a resolvable momentum transfer (q) in the range of 2 to 27 nm^{-1}.

Each sample and the background (residual air) were measured for 700 s under moderate vacuum conditions (10^{-2} mbar pressure) to minimize air scattering. After the measurements, 1D profiles were extracted using DIFFRAC.EVA (Bruker AXS, version 4.1). Transmission corrections and background subtractions were subsequently carried out using an in-house data pipeline running on Matalab R2020b.

The momentum transfer q is related with the scattering angle 2θ through Equation 6 (Equa.6):

$$q = \frac{4\pi}{\lambda} \bullet \sin\left(\frac{2\theta}{2}\right) \quad (6)$$

where λ is the wavelength of the X-ray source [50].

2.15. Microscopic characterization of microfluidic flows and polymer fibers

The flow structures and fiber morphologies were characterized by optical and electron microscopy, respectively. Optical microscopic images were taken with a Leica DMS300, and scanning electric microscopy (SEM, JEOL Hitachi S-4800) images were taken at 2 keV with 7 nm of Au-Pd sputtering on fiber surfaces (EM ACE600, Leica).

2.16. Tensile test of PLA fibers

The mechanical properties of PLA fibers were characterized by using a tensile machine (TS 600, Anton Paar) at room temperature. The gauge length is 10 mm with a tensile speed at 0.40 mm/min. For sample fixation, fibers of typically ~ 1.6 cm long were glued to a plastic platform with a UV sensitive glue (Norland optical adhesive 83H, Norland product), so that the gauge length of 10 mm was ensured. And the plastic platforms were held by clamps of TS 600.

2.17. Cytotoxicity test

Fiber specimens were sterilized by UV radiation (λ = 365 nm), then according to ISO 10993-12 "Biological evaluation of medical devices, Part 12: Sample preparation and reference materials" and ISO 10993-5:2009 "Biological evaluation of medical devices, Part 5: Tests for in vitro cytotoxicity", immersed into complete growth media (DMEM supplemented with 10 % FBS and 1 % P/S) in sterile containers at extraction ratio of 0.1 g/mL for 24 h at 37 °C with continuous, mechanical agitation to obtain the conditioned medium. HDFs (at passages 5 to 9) were plated at 5 000 cells per well in 96-well plates (TPP, Lot. 92096) to a final volume of 100 µL in complete growth media. Cells were cultured for 24 h at 37 °C in 5 % CO_2 to maintain semi-confluent monolayer and then exposed to conditioned medium from different fiber samples. In addition, Cyrene™ solutions in complete media at different concentrations (0.6 – 78 µM) were also used instead of conditioned medium for studying cytotoxicity of Cyrene™. After a 48 h incubation period at 37 °C in 5 % CO_2, all MTT assays were performed using CellTiter 96® Non-Radioactive Cell Proliferation Assay kit according to the manufacturer's manual. Specifically, dye solution (3-(4,5-dimethylthiazol-2-yl)-2,5-diphenyltetrazolium bromide - MTT salt) was dissolved freshly in DMEM (without supplements or phenol red). Absorbance was recorded at 570 nm on a 96 – well plate reader. Percent viability was normalized to cells not exposed to the experimental conditions but cultured in normal complete growth media (negative control). Phenol at 0.25 wt% in the complete growth medium was applied as a positive control.

2.18. Spinning of protein-loaded fibers and characterization of protein release

0.1 wt% Fitc-BSA (A9771-50MG, Sigma-Aldrich) was dissolved in 10 wt% PLA/Cyrene™ solution (freshly cooled down to room temperature after preparation). The prepared spinning dope containing Fitc-BSA was used as core flow, and 2 wt% alginate solution as shell flow for fiber spinning (core flow rate Q_c = 200 µL/min, shell flow rate Q_s = 500 µL/min). The post-spinning treatment was described in section 2.10. For protein release analysis, 75 mg resultant fibers (Fitc-BSA@PLA fibers) were immersed in 15 mL PBS at 37 °C. 2 mL supernatant was taken at each time point (at 0.25 h, 0.5 h, 1 h, 2 h, 4 h, 8 h, 24 h, 30 h and 36 h), and the fluorescent intensity at 510 nm (excitation at 500 nm) was recorded by fluorescent spectrofluorometer (Fluoromax + spectrofluorometer, HORIBA scientific).

2.19. Fabrication of non-woven PLA fiber-based materials

As spun core–shell PLA-Alg fibers were directly collected in predefined molds, where fibers were stacked and subjected to solvent exchange and slow solidification in a DI water bath. After 2 days of solvent exchange, the molded fiber-based materials were taken out from the mold and dried in air.

3. Results and discussions

The selection of proper solvent is a crucial and prerequisite work for microfluidic spinning of polymer fibers [51]. To explore suitable green spinning dope system for PLA, solvent source, toxicity and solubility are important factors to be considered firstly. Compared to other known ε solvents of PLA, Cyrene™ is uniquely bio-based. Its sustainability and low toxicity (high LD50 value) makes it a promising solvent for PLA fiber spinning (Fig. 2**A**) [52–57]. On the one hand, Cyrene™ is considered as a benign solvent of PLA according to the calculation of the Hildebrand solubility parameter (Δδ) and relative energy difference (RED) between Cyrene™ and PLA (Fig. 2**B**). On the other hand, the values of δ_d, δ_p and δ_h for Cyrene™ fall within the range of other known PLA ε solvents (Fig. 2**B**), suggesting that Cyrene™ could induce similar crystallization and gelation behavior of PLA, thus providing a green and pro-crystallization PLA spinning dope.

3.1. Crystallization-induced PLA/ Cyrene™ "sol-gel" transition

To the best of our knowledge, the use of Cyrene™ for dissolving PLA polymers has not been previously reported. Therefore, the investigation of the solution properties of PLA/ Cyrene™ spinning dope is crucial, as it plays an important role in MWS. It was observed that, after being dissolved at 120 °C and cooled down to room temperature, the viscosity of the PLA/ Cyrene™ solution remains stable for ~ 60 min, before gradually reaching a paste-like gel state (Fig. 3**A-B**). To evaluate the detailed PLA/ Cyrene™ "sol-gel" transition, the storage (G') and loss (G'') moduli of the solution were monitored by oscillatory rheological measurements (Fig. 3**B**). Gel formation indicated by the crossover of G'' and G' curves (Gel point) was found at ~ 120 min after the solution was cooled down to room temperature. The paste-like gel can be reverted to the "sol" state by heating at 120 °C for 10 min. The regenerated PLA/ Cyrene™ solution retained the time-dependent gelling property at room temperature within multiple heating–cooling cycles (Supporting Information, **Fig. S2-A**). During the first hour at room temperature, the spinning dope remained a liquid state (G'' < G'), with a slight decrease of G' (from 19.13 Pa to 13.28 Pa) but an increase of G'' (from 0.15 Pa to 2.58 Pa, ~ 17 folds increase) (Supporting information**, Fig. S2-B**). The solution viscosity had no significant changes (less than 7.8 %) in the shear rate range of 0.1–100 s^{-1} (Supporting information, **Fig. S2-C**). After being stored at room temperature for longer periods (1–4 days), the spinning dope can be regenerated by heating to yield a solution of similar viscosity (Supporting information**, Fig. S2-D**).

It was reported that ε solvents could induce the formation of PLA-solvent complex cocrystals, which then act as physical crosslinks and trigger the PLA sol–gel transition [19,58]. The herein discovered fully reversible PLA/Cyrene™ sol–gel transition indicates that Cyrene™

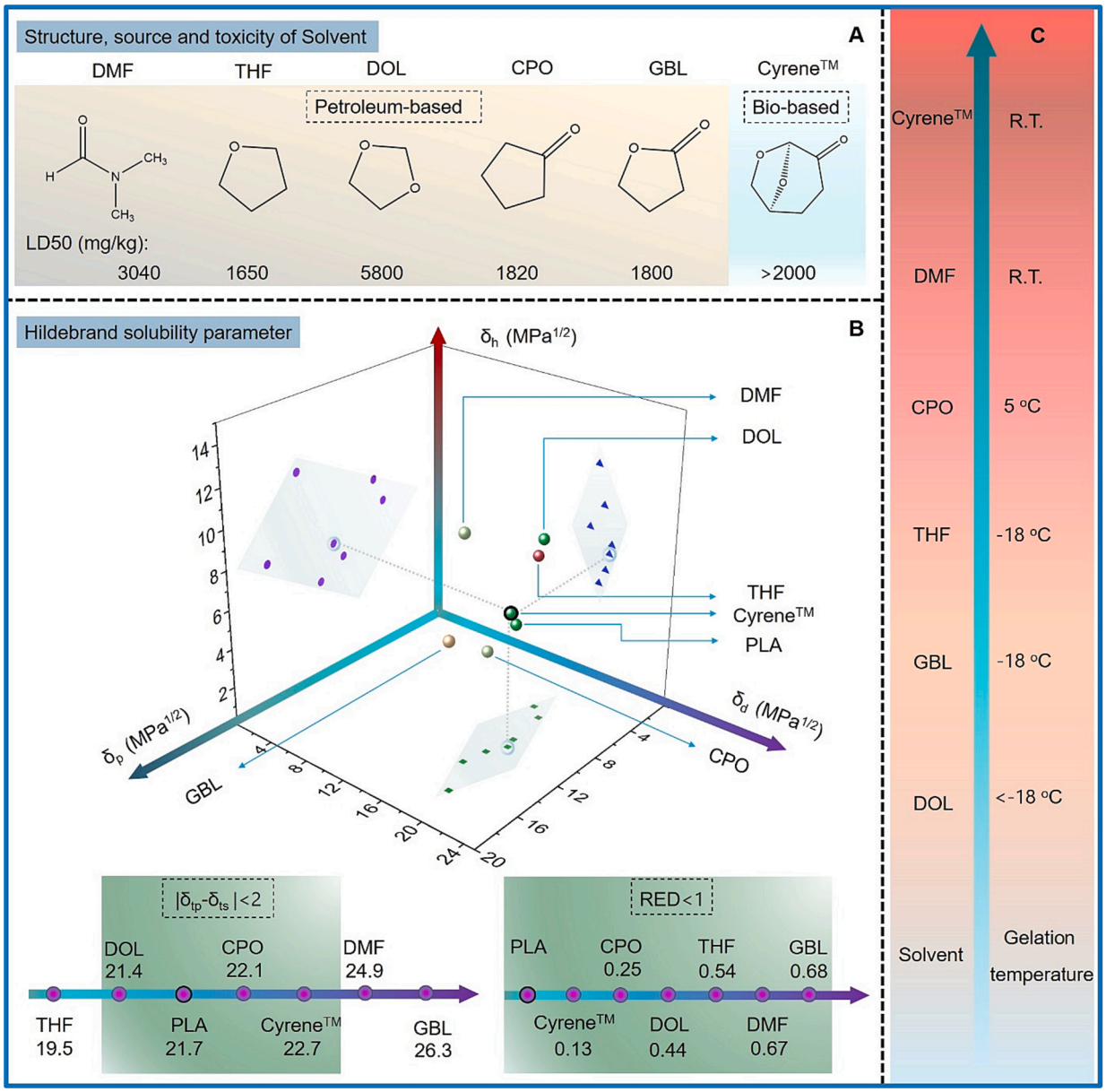

Fig. 2. The comparison between Cyrene™ and other reported ε solvents of PLA. (A) LD50 value of different solvents. (B) Hilderbrand solubility parameter (Δδ) and relative energy difference (RED) of different solvents for PLA. (C) Gelation temperature of PLA solution prepared with different solvents.

could be a green ε solvent for PLA. To reveal the existence of ε form cocrystals, DSC measurements of spinning dope was conducted and an increasing endothermic peak above 60 °C was observed from samples with increasing storage time at room temperature (Fig. 3**C**). The corresponding structural change above glass transition temperature (T_g 55–60 °C, for Ingeo™ Biopolymer 3100HP) was assigned to ε to α transition of PLA crystals (Fig. 3**A**). During this transition, Cyrene™ molecules were expulsed from PLA/Cyrene™ cocrystal lattice to the amorphous phase. This phenomenon was also found in PLA solutions prepared with non-biobased ε solvents, such as cyclopentanone (CPO) [59]. Interestingly, such an ε to α transition was not observed for fresh PLA/Cyrene™ solutions (those stored at room temperature for less than 30 mins. After this initial phase, more PLA/Cyrene™ cocrystals were formed, as revealed by the increasing ε to α transition enthalpy (Supporting information, **Fig. S2 E**).

The solvent induced crystallization in PLA/Cyrene™ spinning dope at room temperature was confirmed with X-ray diffractometry (XRD, Supporting information **Fig. S3 E** and **G**) and polarized optical microscopy (POM, Supporting information **Fig. S3-F**), as well as FTIR spectroscopy (Fig. 3**D,** and Supporting Information **Fig. S3 A-D**). Interestingly, along the "sol-gel" transition process at room temperature, an increase of XRD peaks for α-crystal (2θ =16.6°) was observed. This indicated that some in-situ formed PLA/Cyrene™ ε cocrystals were spontaneously transformed to α-crystals. Meanwhile, FTIR absorbance at 1130 cm^{-1} (asymmetric CH_3 rocking vibrations, Fig. 3**D-i**), 1368 cm^{-1} (symmetric bending of CH and CH_3) and 1457 cm^{-1} (asymmetric bending of CH_3) was observed (Fig. 3**D-iii,** Supporting Information **Fig. S3, C-D**) [60]. Such absorbance increase indicated the increase of PLA crystallinity during the "sol-gel" transition [61,62]. Notably, the band at 1757 cm^{-1} (carbonyl stretching, Fig. 3**D-ii**) related to the formation of PLA left-handed helix was growing during the "sol-gel" transition [63]. In addition, the absorbance at the range of 1375–1395 cm^{-1} (CH_3 symmetric deformation) also increased during "sol-gel" transition (highlighted in dash circle in Fig. 3**D-iii,** Supporting Information **Fig. S3-B**). It was reported that this absorbance band associated with the CH_3 symmetric deformation is sensitive to the PLA chain

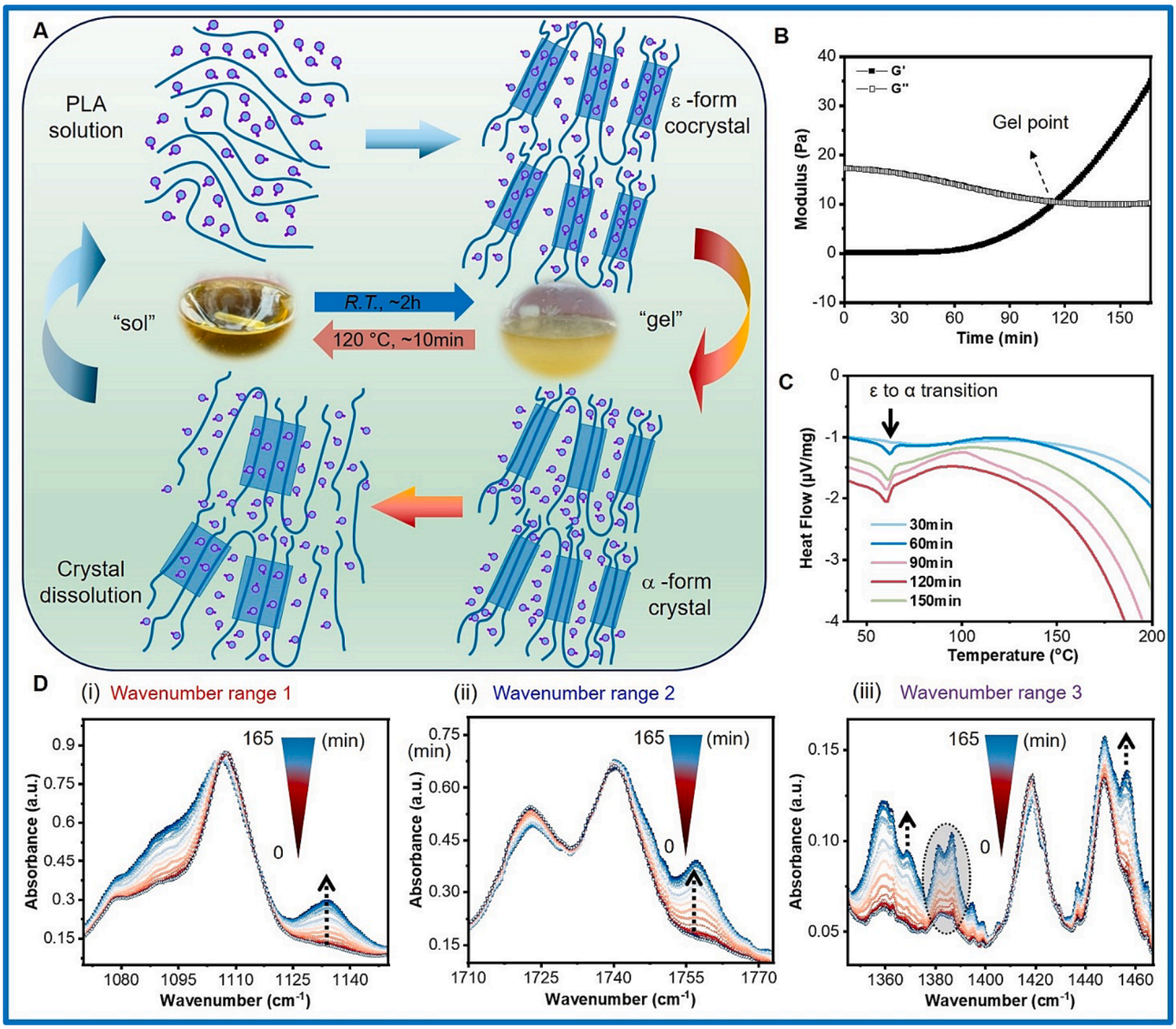

Fig. 3. PLA/Cyrene™ solution properties. **(A)** Digital photos of the PLA/Cyrene™ "sol-gel" transition and the proposed molecular mechanism. **(B)** Oscillatory rheological time-sweep measurement after cooling the PLA/Cyrene™ solution to room temperature. **(C)** DSC measurements of PLA/Cyrene™ solution at different time after cooling to room temperature. **(D)** FTIR spectra of PLA/Cyrene™ solution taken at time points from 0 to 165 min after freshly prepared solution was cooled down to room temperature.

packing.[64] Considering that singlet absorbance peak within this range (at 1383 cm^{-1}) was usually found from α form PLA crystals [59], the herein observed doublet peaks (at 1382 and 1386 cm^{-1}) indicated co-existence of α and ε crystals.

Based on the abovementioned observation, we proposed that in the freshly prepared PLA/Cyrene™ solution, all PLA polymer chains are well solvated and dispersed. After cooling to room temperature, PLA chains partially form helix conformation and induce local aggregation, as evidenced by the FTIR data of the "sol-gel" transition (Fig. 3**D-ii**) [63], which provided space to host Cyrene™ molecules. Such local packing of PLA/Cyrene™ complex gave rise to ill-defined ε-form cocrystals. However, the unstable cocrystals were transformed to the more thermodynamically stable α-crystals at room temperature, as evidenced by the time-resolved XRD study (Supporting information, **Fig. S3 E** and **G**). Such a spontaneous ε-to-α transformation was not complete at PLA/Cyrene™ gel state. The transformation of residual ε-form cocrystals to α-crystals was evidenced by DSC endothermic peak above 60 °C (Fig. 3**C**). This is different from PLA/DMF gels formed at room temperature, which showed no DSC endothermic peak for ε-to-α transformation above 60 °C (Supporting information, **Fig. S2-F**). It was reported that in PLA/DMF system, only α-crystals exist at temperature above 50 °C [19].

3.2. Microfluidic core–shell flow behavior

The PLA/Cyrene™ solution at liquid state was used for MWS of PLA fibers. Its flow behavior in the microfluidic core channel can be controlled by the flow rate conditions (core flow rate Q_c and shell flow rate Q_s) at different concentrations of the shell solution. With a Lego®-based microfluidic setup equipped with coaxial core–shell channels, the flow behavior of PLA/Cyrene™ was investigated by measuring the diameter of the core flow stream (D_{core}) at different flow conditions (Fig. 4**A**).

The selection of a proper shell flow fluid is important for successful fiber spinning. Non-solvents of the polymer are commonly used, since the exchange between non-solvent (in shell flow) and solvent (in core flow) can induce polymer aggregation in the core and thereafter polymer fiber formation. However, general non-solvents for PLA exhibit much lower viscosities than the PLA/Cyrene™ solution. For example, ethanol, a common non-solvent for PLA, has a viscosity of 1.0 mPa·s at

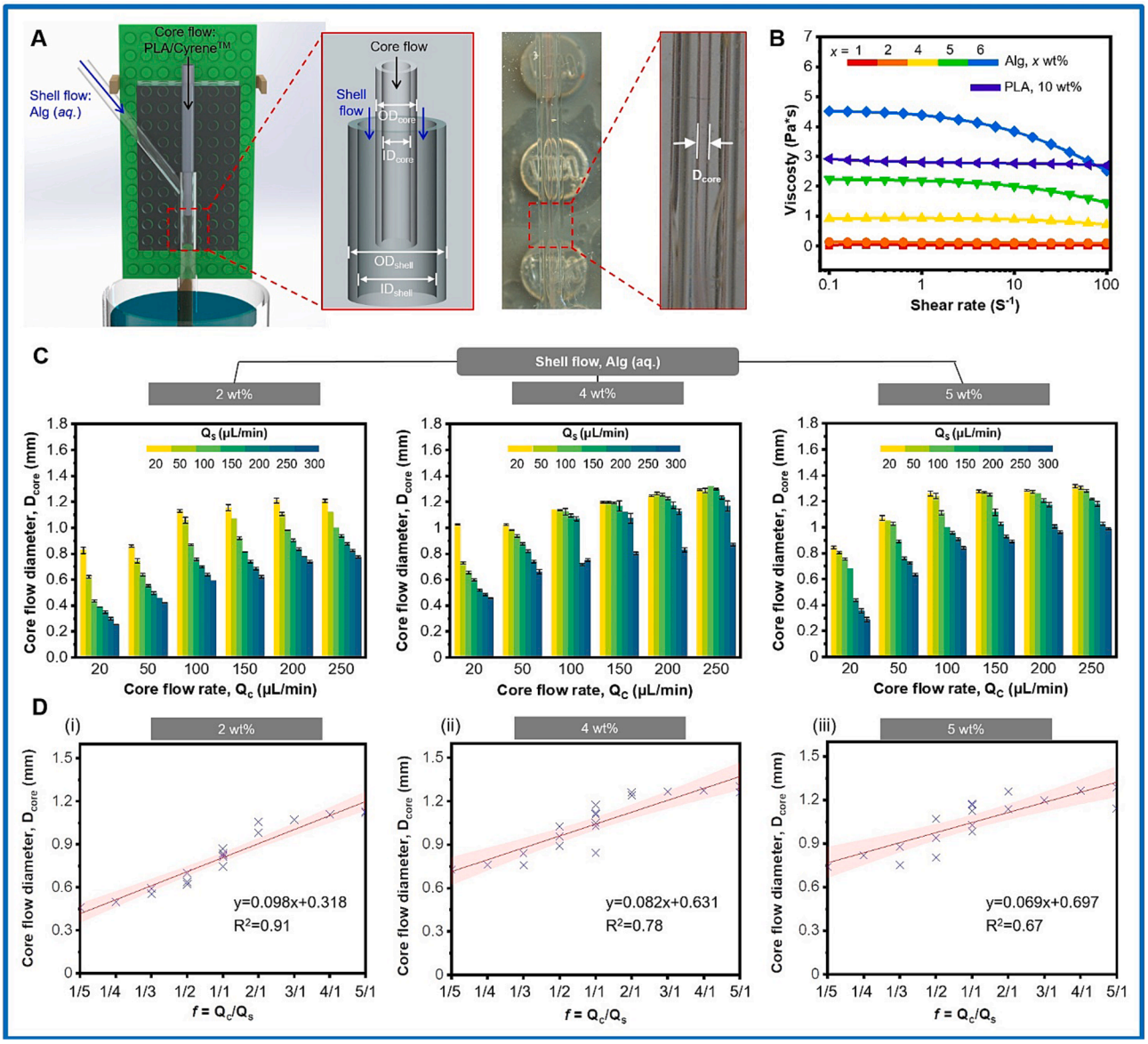

Fig. 4. Flow behavior of PLA/Cyrene™ solution being hydrodynamically shaped by Alg (aq) solution. **(A)** The microfluidic device featuring a coaxial channel configuration, enabling core–shell laminar flow. **(B)** Steady-state viscosity of PLA/Cyrene™ (10 wt%) and Alg (aq) solutions at different concentrations. **(C)** Core flow diameter (D_{core}) under different core–shell flow conditions. **(D)** The relation between core flow diameters (D_{core}) with core–shell flow ratio (Q_c/Q_s).

25 °C [65], much lower than that of PLA/Cyrene™ solution (~3.0 Pa·S, Fig. 4**B**). When ethanol was used as shell flow for PLA solidification, the core–shell viscosity mismatching resulted in unstable flow configurations [66], including unstable continuous core flow, non-disturbed continuous flow, and disturbed continuous flow (Supporting information, **Fig. S4**). Instead of pure non-solvents, Alg (aq) solutions have comparable viscosities to PLA/Cyrene™ solution, and can be adjusted by simply changing concentration (Fig. 4**B**). With a concentration of 2, 4, and 5 wt%, the viscosity of Alg (aq) were 0.123, 0.889, and 2.021 Pa·s (averaged in the shearing rate rage of 0.1–100 s^{-1}), respectively. At each of these three concentrations, the core–shell flow behavior was investigated by measuring the PLA/Cyrene™ core flow diameter (D_{core}, Fig. 4**C**). Overall, at each fixed core flow rate (Q_c), D_{core} can be reduced by increasing the shell flow rate (Q_s). Meanwhile, D_{core} reduction can also be achieved by decreasing Q_c [67,68]. However, this effect in controlling D_{core} is less significant at higher shell flow concentration of Alg (aq), i.e. 4 or 5 wt% (Fig. 4**C**). Hereafter, 2, 4, or 5 wt% Alg (aq) were used as shell flow, lower concentrations were not used, due to the mechanical weakness of the resulting Alg-Ca^{2+} hydrogel shell layer. At 6 wt %, the Alg (aq) is too viscous for maintaining microfluidic flows, therefore, higher concentrations were not used.

It was reported that, for coaxial laminar flow configurations, D_{core} was controlled by the core–shell flow ratio $f = Q_c/Q_s$ with given core and shell solutions (constant viscosities) [32]. This phenomenon was confirmed by analyzing D_{core}-f relations derived from different flow conditions shown in Fig. 4**C**. In particular, with low Alg concentration (i.e. 2 wt%, Fig. 4**D, i**) in shell flow, D_{core} increased linearly with f (R^2 = 0.91). At higher Alg concentrations (i.e. 4 and 5 wt%, Fig. 4**D, ii-iii**), R^2 of the liner fitting decreased to 0.78 and 0.67, respectively. Such a compromise of the linear relationship between D_{core} and f at high Alg concentrations was expected, due to the more profound shear-thinning solution behavior of polymer solutions at higher concentration (Fig. 4**B**). This effect was clearly seen at high Q_s (250 and 300 μL/min), where the shear-induced reduction of apparent Alg viscosity caused the abrupt drop of D_{core} (Fig. 4**D, ii-iii**).

3.3. Hydrogel-assisted fiber spinning

With established core–shell flows as discussed above, PLA fibers can be solidified in core flow via direct solvent exchange, as demonstrated by using Alg (aq) as shell flow without Alg-Ca^{2+} crosslinking (Supporting information, **Fig. S5**). However, PLA fibers spun in this way suffered from poor morphological control and insufficient fiber solidification, as a consequence of the slow core–shell solvent exchange due to the high surface tension, viscosity and polarity of Cyrene™ [69]. Therefore, the hydrogel-assisted microfluidic wet spinning (HA-MWS) method was developed to facilitate extended solvent exchange, so that sufficient fiber solidification can be ensured and uniform fibers can be produced via MWS (Fig. 1**C-F**). Specifically, 0.7 wt% $CaCl_2$ (aq) solution was used as the collection bath, in order to induce the in-situ Alg-Ca^{2+} hydrogel formation, which immediately trapped the solidifying PLA core within the as-formed Alg-Ca^{2+} hydrogel shell, thereby giving rise to the PLA-Alg core–shell fibers. Such fibers can be subjected to extended period of solvent exchange, without compromising the PLA fiber morphologies in the core (Fig. 1**C**). The release of Cyrene™ from the as-spun fibers was investigated by monitoring the release of Cyrene™ into the DI water bath (as describe in Section 2.11) during post-spinning solvent exchange (Fig. 5**A**). UV–Vis absorbance at 230–300 nm indicates the presence of Cyrene™ in the bath, resulted from the solvent exchange (Fig. 5**C**) [70]. Cyrene™ residuals were found in the bath after 1 day of solvent exchange, indicating that the post-spinning PLA solidifying process continued at least for more than 4 h. The removal of Cyrene™ and the solidification was faster when lower Q_c to Q_s ratios were used (e.g. Q_c = 100 μL/min, Q_s = 200 μL/min). To a large extent, this is due to the small core flow diameter (D_{core}) at such spinning conditions, as discussed above in Section 3.2, which facilitates the diffusion of Cyrene™. Nevertheless, for all used spinning conditions, practically all Cyrene™ was extracted within one day at rest in the exchange bath, since the refreshed exchange baths on day two showed negligible Cyrene™ absorbance (Fig. 5**C**, green). As such, the HA-MWS facilitated the removal of solvent, which is necessary for the sufficient solidification of PLA fibers.

The resultant PLA-Alg hybrid fibers were then immersed in sodium chloride solution (NaCl, aq). The competitive binding of Na^+ and Ca^{2+} with Alg caused the dissolution of Alg-Ca^{2+} hydrogel shell, thus yielding pure PLA fibers (Fig. 5**B**). Thermogravimetric analysis (TGA) were used

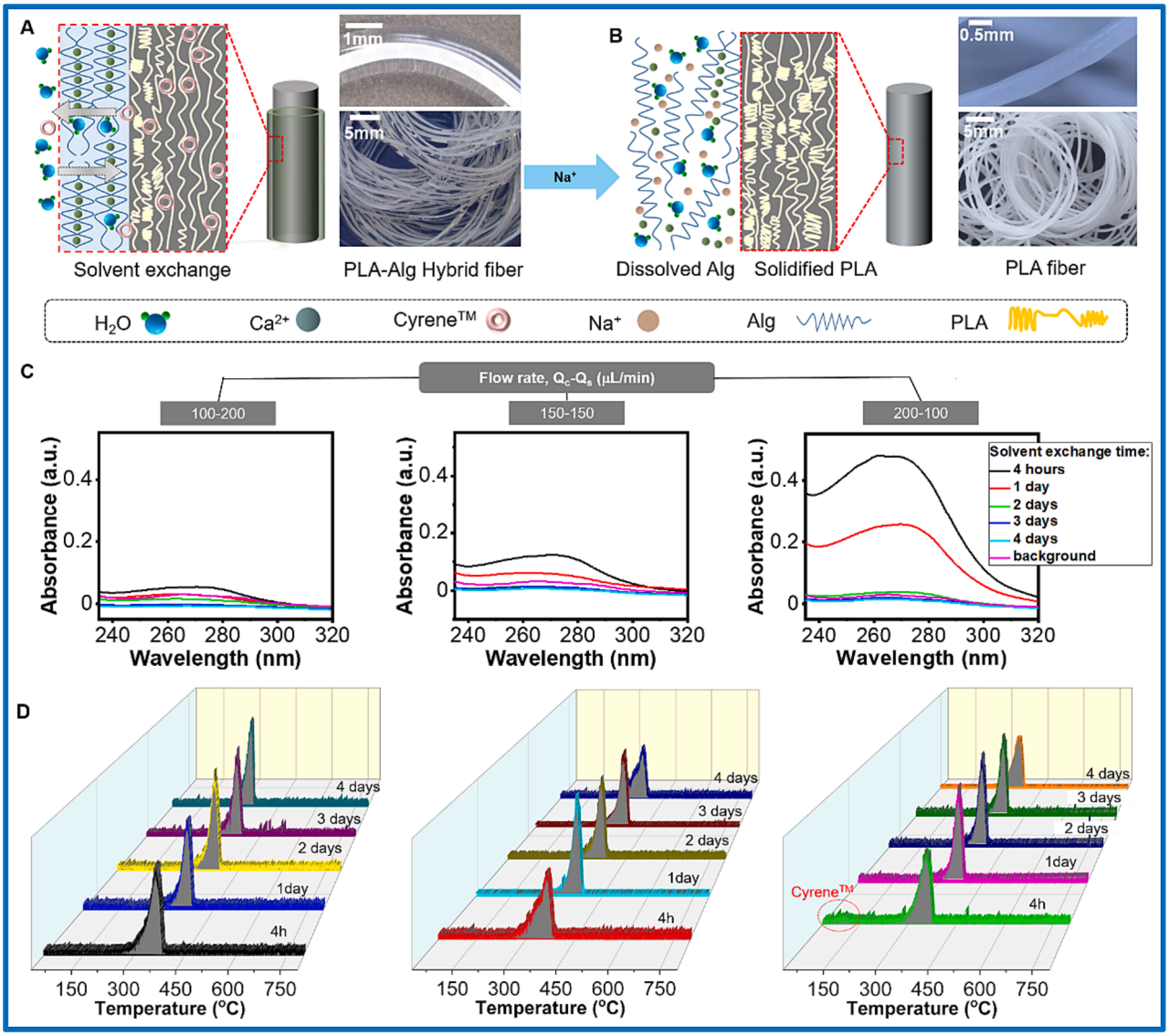

Fig. 5. **(A)** Schematic illustration of solvent exchange between PLA/Cyrene™ core and the DI water bath assisted by the hydrogel shell. **(B)** Hydrogel shell removal after solvent exchange. **(C)** UV–Vis spectra of Cyrene™ released into the refreshing DI water bath. **(D)** DTG spectra of PLA fibers obtained with different solvent exchange time.

to characterize such PLA fibers. To better visualize the weight loss profile, the TGA thermograms (Supporting information, **Fig. S6, A and C**) were processed into derivative thermogravimetry (DTG) curves (Fig. 5**D** and Supporting information, **Fig. S6-B**). PLA fibers obtained after different solvent exchange time were tested with weight loss. No weight loss for PLA fibers produced with extended solvent exchange was observed below 250 °C, except for the one produced with at 200–100 μL/min (Q_c-Q_s) flow condition with 4 h of solvent exchange (Fig. 5**D,** green). In combination with the UV–Vis study, this indicated that 1 day of solvent exchange is enough for removing Cyrene™ residuals and solidifying PLA fibers. In contrast, for fibers produced without refreshing the water bath during solvent exchange, the weight loss at around 100 °C indicated the presence of Cyrene™ residuals (Supporting information, **Fig. S6-B**). In addition, complete removal of alginate hydrogel shells was confirmed by such TGA analysis of the fibers, where no weight loss was observed at 200–280 °C (Fig. 5 and Supporting information, **Fig. S6**) [71].

3.4. PLA fiber structure and mechanical properties

Polymer fiber diameters was reported to be controlled by hydrodynamic focusing, which relies on the flow conditions [67]. The resultant PLA fiber diameters were found in good agreement with such a phenomenon [67]. Specifically, increased fiber diameter (D_{fiber}) can be achieved by adjusting the flow rate condition or the shell flow Alg concentration, as was also found for the change of core flow diameter (D_{core}) (Fig. 6**A**). Representative images of PLA fibers (produced at Q_c-Q_s of 150–150 μL/min) demonstrated the continuous production of PLA-Alg hybrid fibers with PLA core and Alg-Ca^{2+} hydrogel shell (Fig. 6**B-a**). After shell removal, PLA fibers were obtained (Fig. 6**B-b**). The produced PLA fibers have smooth surface and porous inner structures (Supporting information **Table S2**), as revealed by SEM images (Fig. 6**B-c**) [48]. PLA fibers were also produced with different flow rate conditions (Q_c-Q_s of 100–200 and 200–100 μL/min) and shell flow Alg concentrations (2 wt%, 4 wt%, and 5 wt%), which showed uniform morphology (Supporting information, **Fig. S8-S10**). It is noteworthy that, such controlled production of PLA fibers was enabled by the HA-MWS method with Alg solution as a shell flow and cross-linked in-situ into a hydrogel shell. This was not feasible by conventional MWS, where direct solvent exchange is commonly used (Supporting information, **Fig. S5**), or by using conventional ε solvent (e.g. DMF, Supporting information, **Fig. S7**). Fast gelation of PLA/DMF (Fig. S7**A**) allowed only a very short time window (~10 min) for solution-based fiber spinning, making DMF intrinsically less suitable than Cyrene™ for PLA fiber

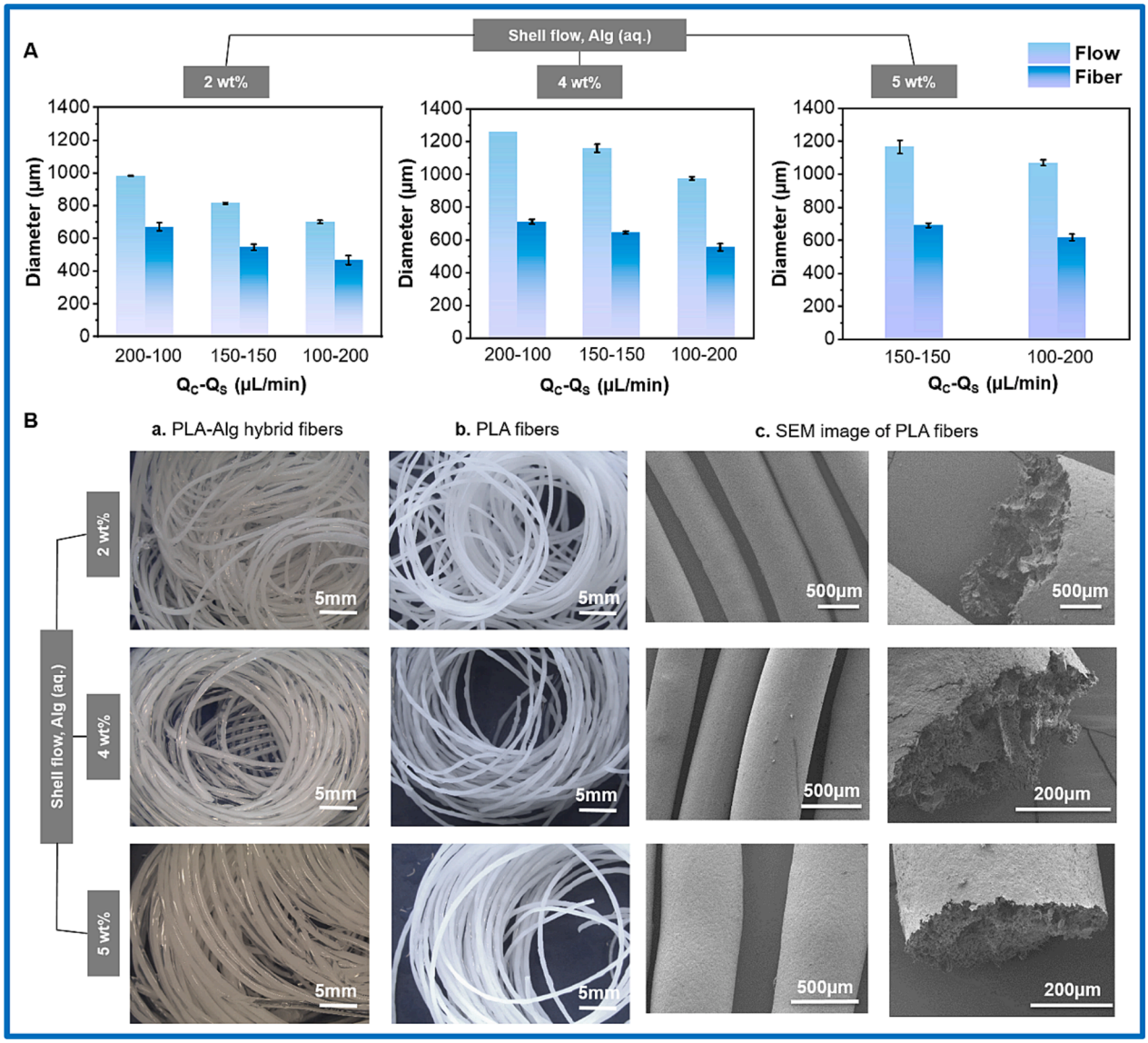

Fig. 6. (A) The diameter of core flows and fibers at different conditions. **(B)** Optical images and SEM images of PLA-Alginate hybrid fibers and PLA fibers.

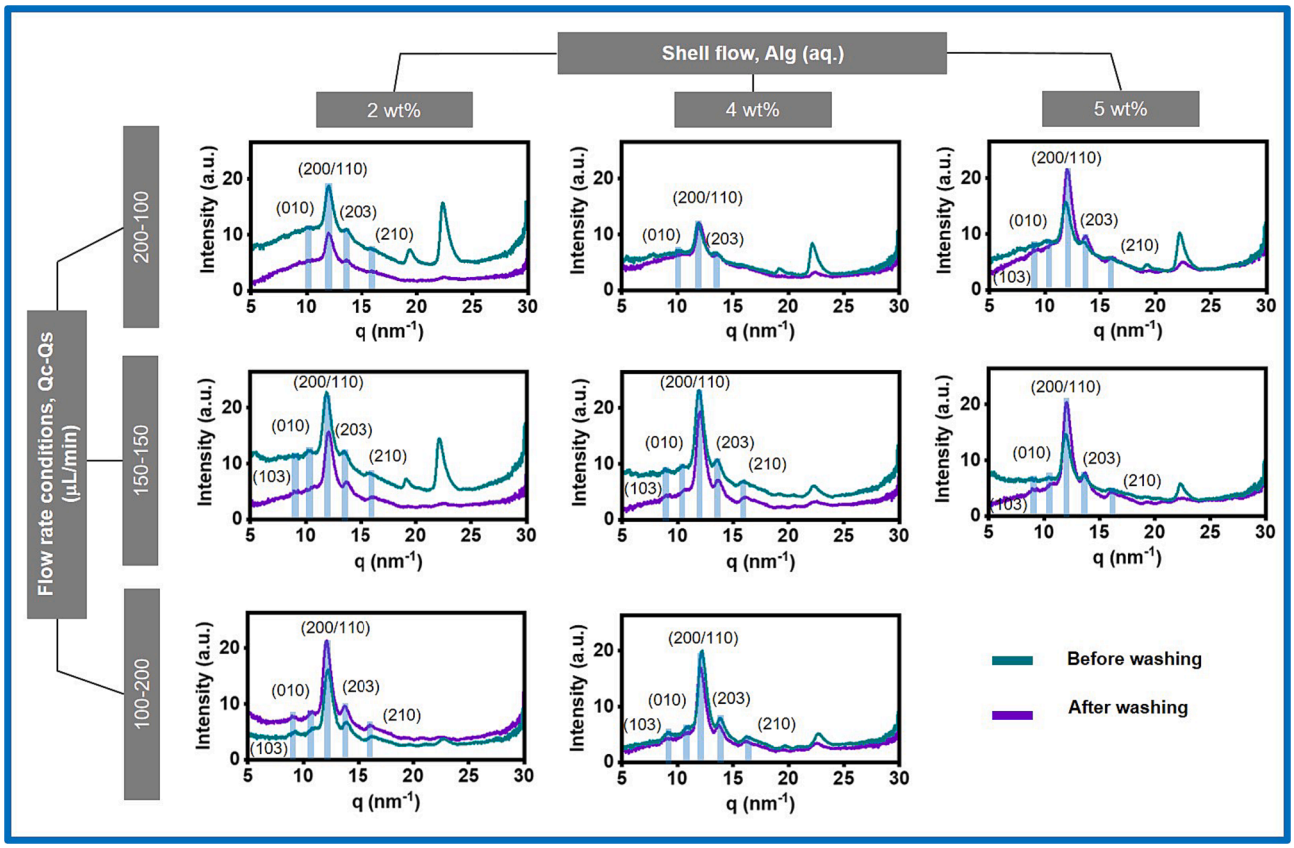

Fig. 7. Characterization of PLA fibers spun under different spinning conditions with XRD (After washing: As-spun PLA fibers were subjected to extended washing with DI water).

spinning. Albeit more challenging, PLA fibers were successfully spun from DMF solution with 2 wt% alginate as shell flow. It is obvious that, PLA/DMF spinning has a less homogeneous core–shell flow, compared to that of PLA/Cyrene^{TM} (Fig. S7**B**). As a consequence, the structure of PLA fibers spun from DMF was not homogeneous (Fig. S7**B**). Therefore, regardless of the similar crystallinity (Fig. S7**D**), tensile strength of PLA fibers spun from DMF solution is too weak to be characterized with our instrument (minimum detectable force 0.05 N).

The internal structure of such PLA fibers was characterized by WAXS. The WAXS profiles (Fig. 7 and Supporting information **Fig. S11**) showed the scattering from typical PLA orthorhombic α-form (200/110) crystal at q = 11.9 nm^{-1} [72]. The prominent crystal plane (200)/(110) peak indicating mass crystallinity is accompanied by (203) and (103) peaks at q = 13.5 nm^{-1} and q = 8.9 nm^{-1}, respectively. Weak peaks of (010) and (210) diffraction (at q = 10.4 nm^{-1} and 15.8 nm^{-1}, respectively) indicates the existence of α'-form crystal, which is a less ordered crystal with poor thermodynamic stability [73,74]. Additional scattering signals at q = 19.1 and 22.1 nm^{-1} were from residual $CaCl_2$ and NaCl salts used in the fiber production process.[75,76] Such signals were reduced by simply washing the PLA fibers in DI water (Fig. 7, after washing).

The degree of PLA crystallinity was calculated from DSC curves. As shown in Fig. 8**A**, the melting peak was observed at ca. 180 °C, corresponding to PLA α-crystals [77]. The crystallinity of these PLA fibers (Fig. 8**B**) was determined by comparing the measured melting enthalpy with the reference melting enthalpy of 100 % crystallinity PLA [78]. The as-produced PLA fibers showed higher degrees of crystallinity (32–46 %) compared to PLA fibers produced with other wet spinning methods without post-spinning treatment (20–30 %) [4,79]. This could be resulted from the pro-crystallization effect of Cyrene^{TM}, which induced the formation of ε-form crystals in the spinning dope. During solvent exchange and fiber solidification, the pre-formed crystals could act as nucleating centers and increased the final PLA crystallinity. It's noteworthy that, cold crystallization signals at 90 °C were not observed for most of the as-produced fibers, except those spun with 2 wt% Alg (aq) as shell flow. This phenomenon is in good agreement with the observed Cyrene^{TM}-induced pre-crystallization in the spinning dope, which lowered or even eliminate the effect of cold crystallization. The as-spun PLA fibers were subsequently characterized with uniaxial tensile testing, giving typical force–elongation curves (Fig. 8**C**). With tensile strength below 2 MPa and elongation at break less than 20 % (Supporting information, **Fig. S12**), the PLA fibers shared common mechanical features with those produced by conventional wet spinning. Especially, the wet-spun fibers show significantly lower tensile strength without post-spinning treatments (e.g. stretching) compared with those fiber with such treatments [80]. The low mechanical strength of wet-spun PLA fibers is mainly due to the porous structures (Fig. 6**B**, Supporting information, Table S2), as a consequence of the solvent exchange process [48]. Such highly porous PLA fibers produced with green spinning dope represents a promising 3D scaffolding materials for tissue engineering applications to support in vitro seeding and culturing of cells [81]. Compared to melt spun PLA fibers that are usually nonporous, the herein-developed fibers could enable sustained release of bioactive elements (such as small molecule drugs and macromolecular growth factors) from the internal pores, thus directing cell growth and differentiation. Furthermore, the large void volume within such fibers holds a great potential to capture and retain the cell-secreted biomolecules and cell-deposited extracellular matrix, thereby promoting in vivo tissue formation.

3.5. *Cytotoxicity test of Cyrene^{TM} and PLA fibers*

Although Cyrene^{TM} has been claimed to have low mutagenicity, no

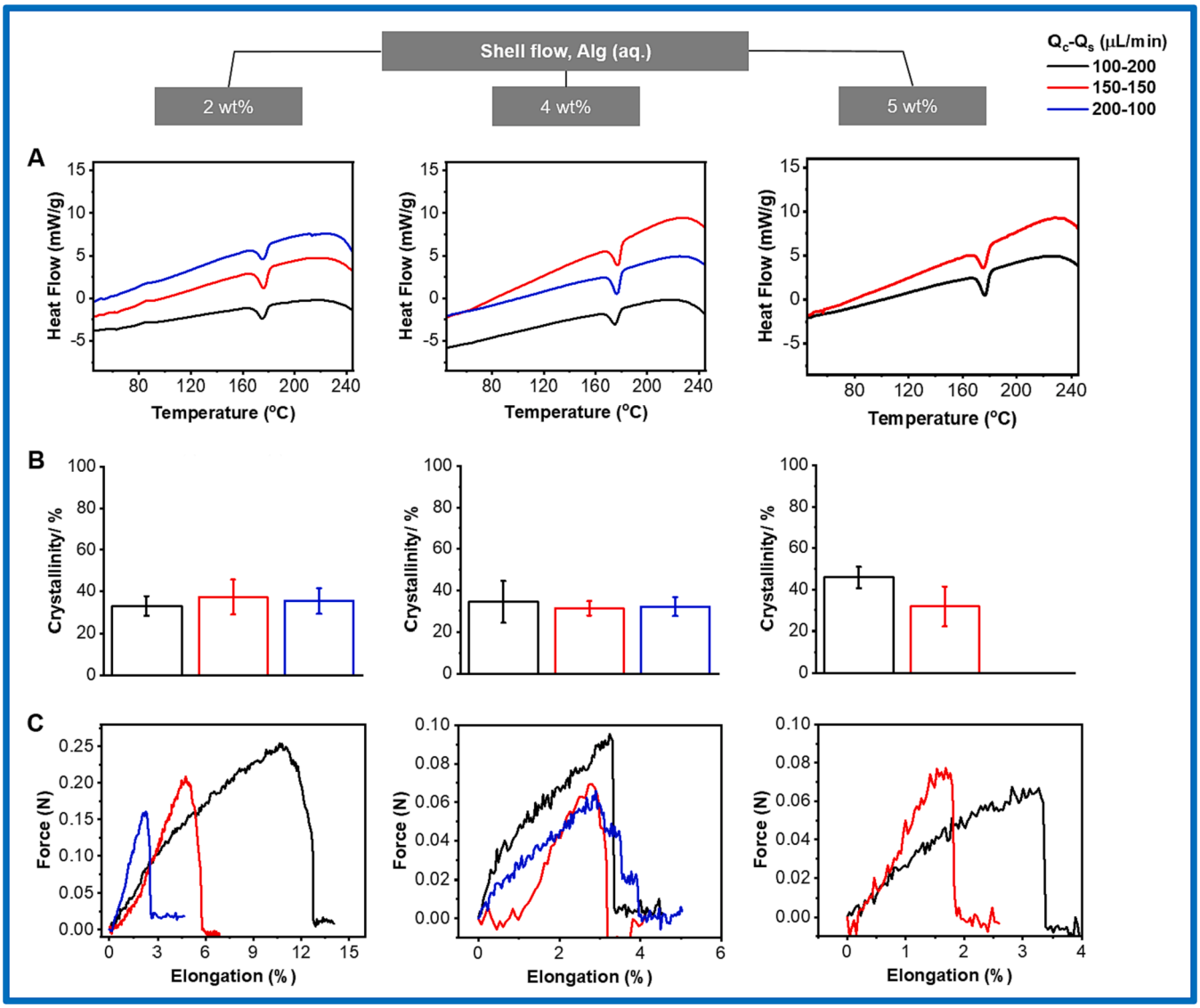

Fig. 8. (A) DSC spectra of PLA fibers spun with different conditions. **(B)** The crystallinity of PLA fibers spun with different conditions. **(C)** The representative force–elongation curves of PLA fibers spun at different conditions.

acute oral toxicity, and low ecotoxicity, and often mentioned as a non-cytotoxic solvent [57,82,83], its concentration dependent toxicity towards human cells was not reported so far. We had tested a range of Cyrene™ concentrations for revealing its toxicity on human dermal fibroblasts (HDF) with MTT assay (Fig. 9**A** and Supporting information **Fig. S12**). Cytotoxic effects were found at the tested concentrations above 6.2 μM (corresponding to 0.08 wt%). Interestingly, at lower tested concentrations, i.e. 4.7–1.6 μM, Cyrene™ was found to promote cell proliferation, as indicated by the higher cell viability than the negative (neg.) control group (cultured in normal medium). By virtue of extended solvent exchange process enabled by HA-MWS, Cyrene™ can be thoroughly removed from PLA fibers produced from PLA/Cyrene™ green spinning dope. Therefore, such PLA fibers were expected to have excellent cytocompatibility. PLA fibers spun with three representative conditions were subjected to cytotoxicity study according to ISO 10993-"Biological Evaluation of Medical Devices" (Fig. 9**B**). Cell viabilities (normalized to negative group) were found above 100 % from all three groups (Fig. 9**B**). Cells cultured in the conditioning media containing PLA fiber extracts were found in elongated and spreading state, confirming the good cytocompatibility of PLA fibers (Fig. 9**C**). Such a pro-cell-growth effect could be ascribed to the residual Cyrene™ molecules within the fibers, which were of too low amount to be detected by TGA characterization (Fig. 5), but had a positive impact on cell growth.

3.6. Fabrication of non-woven PLA fiber-based wound dressing materials

While the nontoxic nature of the PLA fibers fulfills the basic requirement for various biomedical applications, the highly porous feature (above 80 %, Supporting information, Table S2) and mild spinning condition (i.e. room temperature, green solvent, water-based solvent-exchange) enables direct fabrication of bioactive PLA fibers for wound dressing (by dissolving bioactive compounds such as proteins and growth factors in the green spinning dope). As a proof-of-concept, a fluorescence-labeled model protein (Fitc-BSA) was loaded in PLA fibers (Fig. 10**A**). The sustained release of proteins was demonstrated within 36 h in PBS at 37 °C (Fig. 10**B**). This makes the porous PLA fibers promising for bioactive wound dressings, where mechanical strength is not a critical requirement (which can be often mechanically supported by backing medical textiles or other materials in practices). The preservation and sustained release of bioactive compounds into the harsh microenvironments of chronic wounds could increase the therapeutic

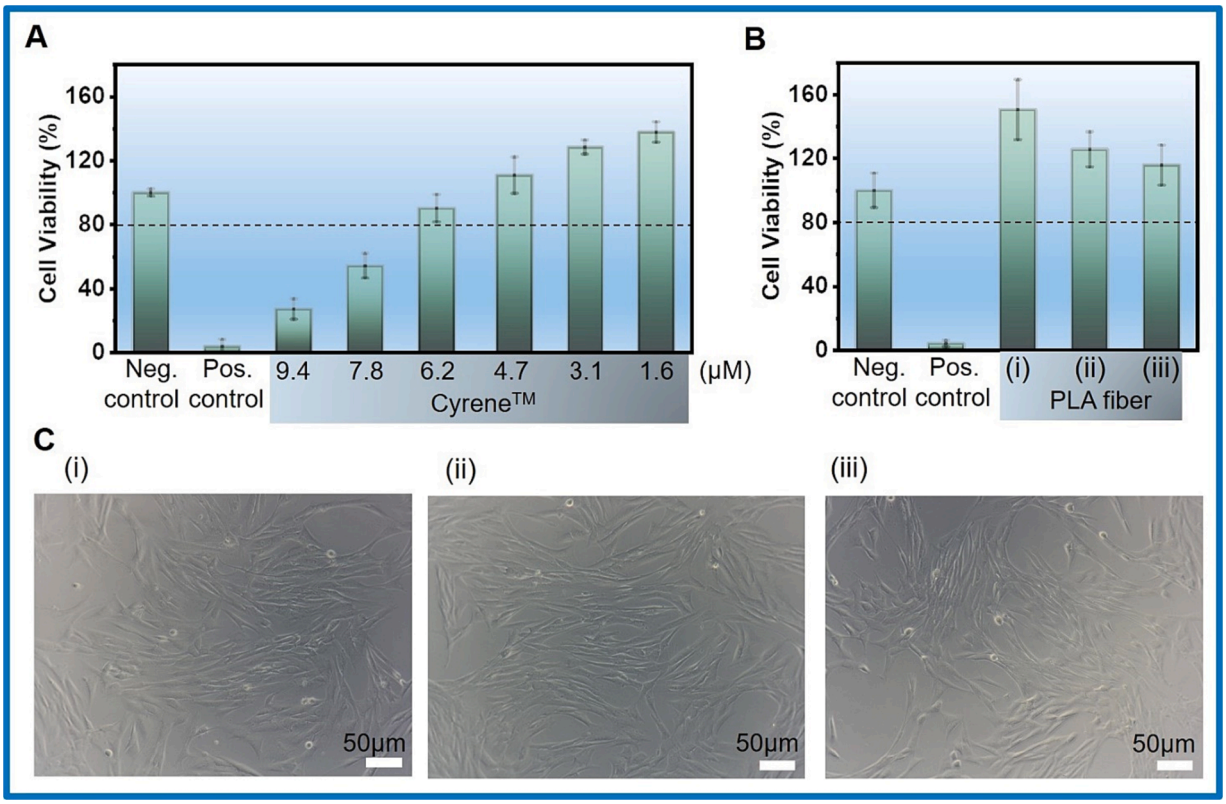

Fig. 9. Viability of HDF p5-p7 juvenile pool cells cultured at different Cyrene™ concentrations in culture media for 24 h **(A)**, or in conditioned media from PLA fibers spun at different Q_c-Q_s conditions with 2 wt% Alg solution as shell flow **(B)**. **(C)** Representative microscopic images of cells cultured with PLA fiber conditioned media after 24 h. PLA fiber spinning conditions were (i) 100–200 μL/min, (ii) 150–150 μL/min; (iii) 200–100 μL/min).

efficiency, thus promoting wound healing.

Furthermore, owing to the slow solidification enabled by our HA-MWS strategy, the as-spun fibers could be facilely made into non-woven fiber-based shape-adaptive materials, as shown in Fig. 10**C-D**, making it particularly attractive in wound dressing for non-flat body parts, e.g. whole finger. In combination with the protein-loading and sustained release properties, the PLA fibers produced via HA-MWS showed a great promise in chronic wound management.

4. Conclusion

In conclusion, we established a green and pro-crystallization spinning dope for PLA fiber production via a novel hydrogel-assisted microfluidic wet spinning (HA-MWS) strategy. Cyrene™, the selected bio-based solvent, was discovered as the first bio-based green solvent for inducing PLA crystallization and "sol-gel" transition, and used for the first time in microfluidic wet spinning of polymer fibers. The unique features of the Cyrene™-based PLA spinning dope include the fully reversible "sol-gel" transition, formation of PLA gel at room temperature (not feasible for most known PLA ε solvents, Fig. 2), as well as the excellent cytocompatibility of resultant PLA fibers. By exploring the novel PLA/Cyrene™ spinning dope with biopolymer (alginate) hydrogels, PLA fibers with smooth surface, porous internal structure and high crystallinity were produced in a way fully independent from petroleum-based solvents. This was made possible by the development of the HA-MWS strategy, where the in-situ formed temporal hydrogel-shell allows controlled solvent exchange and fiber solidification process under mild conditions (e.g., room temperature, water-based post-spinning treatments). This not only provides a green and sustainable option for PLA fiber production, but also enables other post-spinning treatment of the solidifying PLA fibers during the extended solvent exchange time. Such treatment could include in-situ drawing of the semi-solidified PLA core, which can lead to improved mechanical strength due to the macromolecular and crystal alignment. The extended solvent exchange process at room temperature would also provide opportunities for post-spinning functionalization by loading bioactive compounds (e.g. small molecule drugs and macromolecular growth factors). Compared to melt spun PLA fibers that are usually nonporous, regardless of the relatively weak mechanical strength, the herein-developed fibers could therefore enable sustained release of bioactive elements from the internal pores to direct cell growth and differentiation, which makes it attractive wound dressing materials, as well as scaffolding materials for in vitro cell culture, tissue engineering, and so-called "organ-weaving" applications [81].

CRediT authorship contribution statement

Wuchao Wang: Conceptualization, Investigation, Writing – original draft, Writing – review & editing, Data curation, Formal analysis, Methodology, Visualization. **Jonathan Avaro:** Investigation, Data curation, Writing – review & editing. **Tobias Hammer:** Investigation, Validation, Writing – review & editing. **Lucyna Hämmerle:** Investigation, Data curation, Writing – review & editing. **Bruno F. B. Silva:** Investigation, Resources, Writing – review & editing. **Luciano F. Boesel:** Investigation, Formal analysis, Funding acquisition, Writing – review & editing. **René M. Rossi:** Investigation, Supervision, Conceptualization, Funding acquisition, Validation, Writing – review & editing. **Kongchang Wei:** Conceptualization, Investigation, Writing – original draft, Writing – review & editing, Formal analysis, Methodology, Project administration, Supervision, Validation, Visualization.

Declaration of competing interest

The authors declare that they have no known competing financial

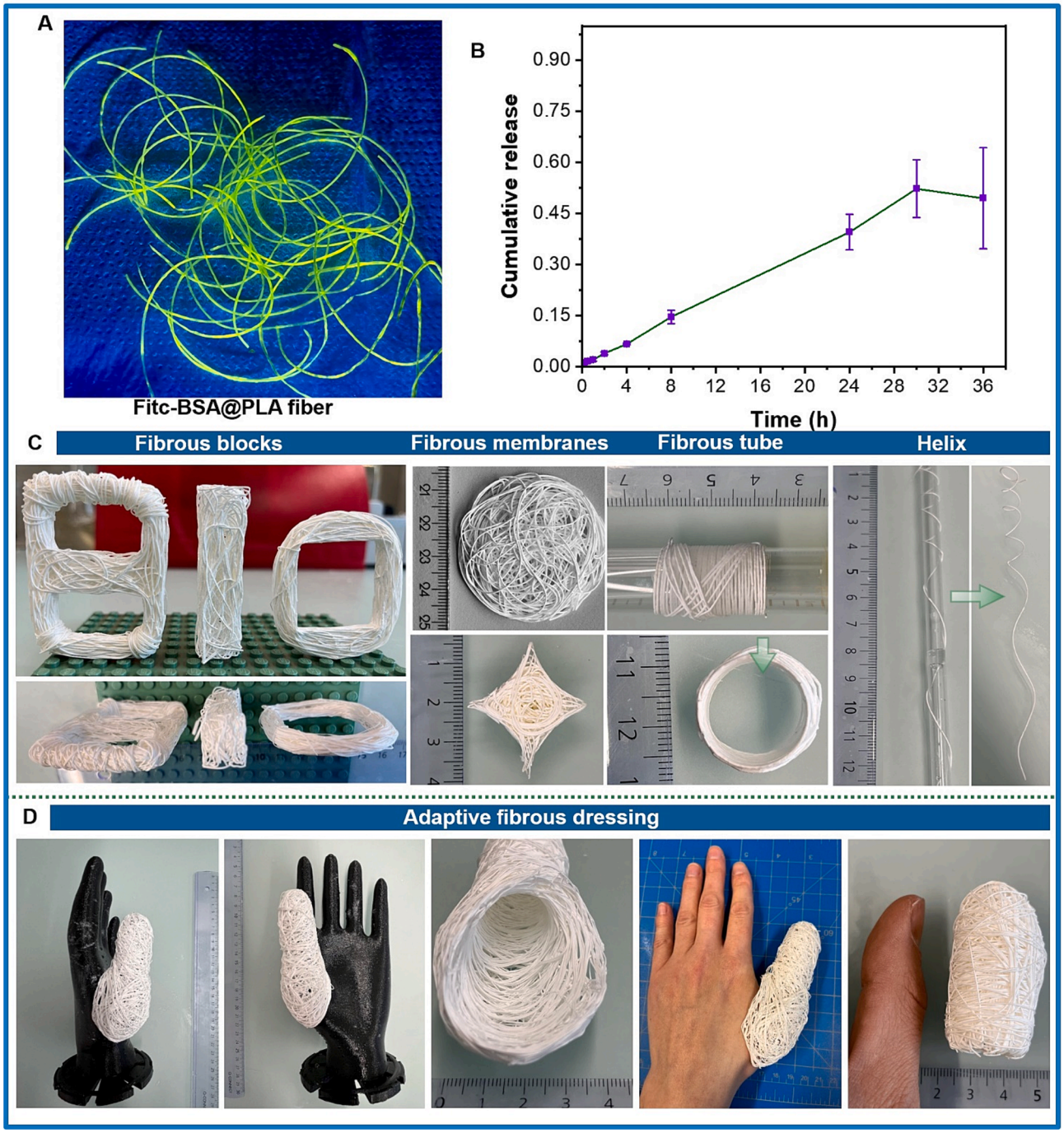

Fig. 10. **(A)** A digital photo of PLA fibers with Fitc-BSA directly encapsulated during HA-MWS. **(B)** Sustained release of Fitc-BSA from PLA fibers into PBS. Fibrous blocks and membranes **(C)** were produced by solidifying fibers in moulds. Fibrous tube, helix and dressing **(D)** were fabricated by warping.

interests or personal relationships that could have appeared to influence the work reported in this paper.

Data availability

Data will be made available on request.

Acknowledgements

The author Wang W. acknowledges China Scholar Council (CSC) for the scholarship (CSC number:202006990009). The project was supported by the Swiss National Science Foundation (SNSF) and Innosuisse BRIDGE Discovery funding opportunity (project number 40B2-0_180983, ProTex), as well as the Subitex research initiative (Switzerland). The authors thank Dr. Michael Dieter Wörle for helping with XRD characterizations.

Appendix A. Supplementary data

Supplementary data to this article can be found online at https://doi.org/10.1016/j.cej.2023.148417.

References

[1] P.T. Benavides, U. Lee, O. Zarè-Mehrjerdi, Life cycle greenhouse gas emissions and energy use of polylactic acid, bio-derived polyethylene, and fossil-derived polyethylene, J. Cleaner Prod. 277 (2020) e124010.

[2] P. Majgaonkar, R. Hanich, F. Malz, R. Brüll, Chemical Recycling of Post-Consumer PLA Waste for Sustainable Production of Ethyl Lactate, Chem. Eng. J. 423 (2021) e129952.

[3] V. DeStefano, S. Khan, A. Tabada, Applications of PLA in modern medicine, Eng. Regener. 1 (2020) 76–87, https://doi.org/10.1016/j.engreg.2020.08.002.

[4] B. Gupta, N. Revagade, J. Hilborn, Poly(lactic acid) fiber: An overview, Prog. Polym. Sci. 32 (4) (2007) 455–482, https://doi.org/10.1016/j.progpolymsci.2007.01.005.

[5] Y. Li, Q. Meng, S. Chen, P. Ling, M.A. Kuss, B. Duan, S. Wu, Advances, challenges, and prospects for surgical suture materials, Acta Biomater. 168 (2023) 78–112, https://doi.org/10.1016/j.actbio.2023.07.041.

[6] B. Li, Z. Xie, Q. Wang, X. Chen, Q. Liu, W. Wang, Y. Shen, J. Liu, A. Li, Y. Li, G. Zhang, J. Liu, D. Zhang, C. Liu, S. Wang, Y. Xie, Z. Zhang, J. Ding, Biodegradable polymeric occluder for closure of atrial septal defect with interventional treatment of cardiovascular disease, Biomaterials 274 (2021) e120851.

[7] B. Zhang, L. Wang, P. Song, X. Pei, H. Sun, L. Wu, C. Zhou, K. Wang, Y. Fan, X. Zhang, 3D printed bone tissue regenerative PLA/HA scaffolds with comprehensive performance optimizations, Mater. Des. 201 (2021) e109490.

[8] T.T. Ngo, P.J. Waggoner, A.A. Romero, K.D. Nelson, R.C. Eberhart, G.M. Smith, Poly(L-Lactide) microfilaments enhance peripheral nerve regeneration across extended nerve lesions, J. Neurosci. Res. 72 (2) (2003) 227–238, https://doi.org/10.1002/jnr.10570.

[9] B. Gupta, and Nilesh Revagade, Development and structural evaluation of poly (lactic acid) based knitted scaffold for human urinary bladder reconstruction, Indian J. Fiber Text. Res. 34 (2009) 115–121.

[10] S. Liu, S. Qin, M. He, D. Zhou, Q. Qin, H. Wang, Current applications of poly(lactic acid) composites in tissue engineering and drug delivery, Compos. b: Eng. 199 (2020) e108238.

[11] .W. Cheung, Creation of Smart Wearable Textile-based Drug Delivery System with the use of hollow fibers, The Hong Kong Polytechnic University, 2019.

[12] L.T. Lim, R. Auras, M. Rubino, Processing technologies for poly(lactic acid), Prog. Polym. Sci. 33 (8) (2008) 820–852, https://doi.org/10.1016/j.progpolymsci.2008.05.004.

[13] E. Castro-Aguirre, F. Iniguez-Franco, H. Samsudin, X. Fang, R. Auras, Poly(lactic acid)-Mass production, processing, industrial applications, and end of life, Adv. Drug Deliv. Rev. 107 (2016) 333–366, https://doi.org/10.1016/j.addr.2016.03.010.

[14] C.R. Gajjar, J.W. Stallrich, M.A. Pasquinelli, M.W. King, Process-Property Relationships for Melt-Spun Poly(lactic acid) Yarn, ACS Omega 6 (24) (2021) 15920–15928, https://doi.org/10.1021/acsomega.1c01557.

[15] Y. Yang, M. Zhang, Z. Ju, P.Y. Tam, T. Hua, M.W. Younas, H. Kamrul, H. Hu, Poly (lactic acid) fibers, yarns and fabrics: Manufacturing, properties and applications, Text. Res. J. 91 (13–14) (2020) 1641–1669, https://doi.org/10.1177/0040517520984101.

[16] D.M. Lavin, L. Zhang, S. Furtado, R.A. Hopkins, E. Mathiowitz, Effects of protein molecular weight on the intrinsic material properties and release kinetics of wet spun polymeric microfiber delivery systems, Acta Biomater. 9 (1) (2013) 4569–45678, https://doi.org/10.1016/j.actbio.2012.08.005.

[17] D.M. Lavin, R.M. Stefani, L. Zhang, S. Furtado, R.A. Hopkins, E. Mathiowitz, Multifunctional polymeric microfibers with prolonged drug delivery and structural support capabilities, Acta Biomater. 8 (5) (2012) 1891–1900, https://doi.org/10.1016/j.actbio.2012.01.019.

[18] M.R. Jung, I.K. Shim, E.S. Kim, Y.J. Park, Y.I. Yang, S.K. Lee, S.J. Lee, Controlled release of cell-permeable gene complex from poly(L-lactide) scaffold for enhanced stem cell tissue engineering, J. Control Release 152 (2) (2011) 294–302, https://doi.org/10.1016/j.jconrel.2011.03.002.

[19] N.M. Praveena, N.S. Akhila, E. Bhoje Gowd, Polylactide cocrystals and gels, SPE Polymers 4 (1) (2023) 3–15, https://doi.org/10.1002/pls2.10083.

[20] M. Giełdowska, M. Puchalski, S. Sztajnowski, I. Krucińska, Evolution of the Molecular and Supramolecular Structures of PLA during the Thermally Supported Hydrolytic Degradation of Wet Spinning Fibers, Macromolecules 55 (22) (2022) 10100–10112, https://doi.org/10.1021/acs.macromol.2c01778.

[21] H. Gao, Y. Gu, Q. Ping, The implantable 5-fluorouracil-loaded poly(l-lactic acid) fibers prepared by wet-spinning from suspension, J. Control Release 118 (3) (2007) 325–332, https://doi.org/10.1016/j.jconrel.2006.12.028.

[22] R.C.C. Domingues, C.C. Pereira, C.P. Borges, Morphological control and properties of poly(lactic acid) hollow fibers for biomedical applications, J. Appl. Polym. Sci. 134 (47) (2017) e45494.

[23] C. Fabris, D. Perin, G. Fredi, D. Rigotti, M. Bortolotti, A. Pegoretti, E. Xanthopoulou, D.N. Bikiaris, A. Dorigato, Improving the Wet-Spinning and Drawing Processes of Poly(lactide)/Poly(ethylene furanoate) and Polylactide/Poly (dodecamethylene furanoate) Fiber Blends, Polymers (Basel) 14(14) (2022) e2910. Doi: 10.3390/polym14142910.

[24] W. Han, D. Rao, H. Gao, X. Yang, H. Fan, C. Li, L. Dong, H. Meng, Green-solvent-processable biodegradable poly(lactic acid) nanofibrous membranes with bead-on-string structure for effective air filtration: "Kill two birds with one stone, Nano Energy 97 (2022) e107237.

[25] A. Tampau, C. Gonzalez-Martinez, A. Chiralt, Polylactic acid-based materials encapsulating carvacrol obtained by solvent casting and electrospinning, J. Food Sci. 85 (4) (2020) 1177–1185, https://doi.org/10.1111/1750-3841.15094.

[26] A. Salerno, C. Domingo, Making microporous nanometre-scale fibrous PLA aerogels with clean and reliable supercritical CO2 based approaches, Microporous Mesoporous Mater. 184 (2014) 162–168, https://doi.org/10.1016/j.micromeso.2013.10.019.

[27] C. Yang, F. Topuz, S.-H. Park, G. Szekely, Biobased thin-film composite membranes comprising priamine–genipin selective layer on nanofibrous biodegradable polylactic acid support for oil and solvent-resistant nanofiltration, Green Chem. 24 (13) (2022) 5291–5303, https://doi.org/10.1039/d2gc01476a.

[28] S.T. Sikhosana, T.P. Gumede, N.J. Malebo, A.O. Ogundeji, Poly(lactic acid) and its composites as functional materials for 3-D scaffolds in biomedical applications: A mini review of recent trends, Express Polym. Lett. 15 (6) (2021) 568–580, https://doi.org/10.3144/expresspolymlett.2021.48.

[29] A. Luken, M. Geiger, L. Steinbeck, A.C. Joel, A. Lampert, J. Linkhorst, M. Wessling, Biocompatible Micron-Scale Silk Fibers Fabricated by Microfluidic Wet Spinning, Adv. Healthc. Mater. 10 (20) (2021) e2100898.

[30] K. Wei, C. Toncelli, R.M. Rossi, L.F. Boesel, Hydrogel Fibers Produced via Microfluidics, in: R.A. Pires, I. Pashkuleva, R.L. Reis (Eds.), Multifunctional Hydrogels for Biomedical Applications, Wiley-VCH GmbH, 2022, pp. 233–274.

[31] D. Li, M.M. Jacobsen, N. Gyune Rim, D. Backman, D.L. Kaplan, J.Y. Wong, Introducing biomimetic shear and ion gradients to microfluidic spinning improves silk fiber strength, Biofabrication 9 (2) (2017) e025025.

[32] X.Y. Du, Q. Li, G. Wu, S. Chen, Multifunctional Micro/Nanoscale Fibers Based on Microfluidic Spinning Technology, Adv. Mater. 31 (52) (2019) e1903733.

[33] X. Hu, M. Tian, B. Sun, L. Qu, S. Zhu, X. Zhang, Hydrodynamic alignment and microfluidic spinning of strength-reinforced calcium alginate microfibers, Mater. Lett. 230 (2018) 148–151, https://doi.org/10.1016/j.matlet.2018.07.092.

[34] Y. Yang, D. Chen, Y. Cheng, B. Sun, G. Zhao, W. Fei, W. Han, J. Han, X. Zhang, Eco-friendly and sustainable approach of assembling sugars into biobased carbon fibers, Green Chem. 24 (13) (2022) 5097–5106, https://doi.org/10.1039/d2gc01075e.

[35] J. Wang, Q. Gao, Y. Wang, X. Liu, S. Nie, Strong fibrous filaments nanocellulose crystals prepared by self-twisting microfluidic spinning, Ind. Crops Prod. 178 (2022) e114599.

[36] C.J. Clarke, W.C. Tu, O. Levers, A. Brohl, J.P. Hallett, Green and Sustainable Solvents in Chemical Processes, Chem. Rev. 118 (2) (2018) 747–800, https://doi.org/10.1021/acs.chemrev.7b00571.

[37] J. Sherwood, M. De bruyn, A. Constantinou, L. Moity, C.R. McElroy, T.J. Farmer, T. Duncan, W. Raverty, A.J. Hunt, J.H. Clark, Dihydrolevoglucosenone (Cyrene) as a bio-based alternative for dipolar aprotic solvents, Chem. Commun. 50(68) (2014) 9650-9652. Doi: 10.1039/c4cc04133j.

[38] N.A. Stini, P.L. Gkizis, C.G. Kokotos, Cyrene: a bio-based novel and sustainable solvent for organic synthesis, Green Chemistry 24 (17) (2022) 6435–6449, https://doi.org/10.1039/d2gc02332f.

[39] F.P. Byrne, S. Jin, G. Paggiola, T.H.M. Petchey, J.H. Clark, T.J. Farmer, A.J. Hunt, C. Robert McElroy, J. Sherwood, Tools and techniques for solvent selection: green solvent selection guides, Sustainable Chem. Processes 4(1) (2016) 1-24. Doi: 10.1186/s40508-016-0051-z.

[40] C. Sullivan, Y. Zhang, G. Xu, L. Christianson, F. Luengo, T. Halkoski, P. Gao, Cyrene™ blends: a greener solvent system for organic syntheses, Green Chem. 24 (18) (2022) 7184–7193, https://doi.org/10.1039/d2gc01911f.

[41] T. Marino, F. Galiano, A. Molino, A. Figoli, New frontiers in sustainable membrane preparation: Cyrene™ as green bioderived solvent, J. Membr. Sci. 580 (2019) 224–234, https://doi.org/10.1016/j.memsci.2019.03.034.

[42] R.A. Milescu, C.R. McElroy, T.J. Farmer, P.M. Williams, M.J. Walters, J.H. Clark, Fabrication of PES/PVP Water Filtration Membranes Using Cyrene®, a Safer Bio-Based Polar Aprotic Solvent, Adv. Polym. Technol. 2019 (2019) 1–15, https://doi.org/10.1155/2019/9692859.

[43] P. Tomietto, F. Russo, F. Galiano, P. Loulergue, S. Salerno, L. Paugam, J.L. Audic, L. De Bartolo, A. Figoli, Sustainable fabrication and pervaporation application of bio-based membranes: Combining a polyhydroxyalkanoate (PHA) as biopolymer and Cyrene™ as green solvent, J. Membr. Sci. 643 (2022) e120061.

[44] C. Grune, J. Thamm, O. Werz, D. Fischer, Cyrene as an Alternative Sustainable Solvent for the Preparation of Poly(lactic-co-glycolic acid) Nanoparticles, J. Pharm. Sci. 110 (2) (2021) 959–964, https://doi.org/10.1016/j.xphs.2020.11.031.

[45] J. Fernandes, S.S. Nemala, G. De Bellis, A. Capasso, Green Solvents for the Liquid Phase Exfoliation Production of Graphene: The Promising Case of Cyrene, Front. Chem. 10 (2022) e878799.

[46] A. Agrawal, A.D. Saran, S.S. Rath, A. Khanna, Constrained nonlinear optimization for solubility parameters of poly(lactic acid) and poly(glycolic acid)—validation and comparison, Polymer 45 (25) (2004) 8603–8612, https://doi.org/10.1016/j.polymer.2004.10.022.

[47] H. Marubayashi, S. Asai, M. Sumita, Guest-induced crystal-to-crystal transitions of poly(L-lactide) complexes, J. Phys. Chem. B 117 (1) (2013) 385–397, https://doi.org/10.1021/jp308999t.

[48] A. Gursoy, K. Iranshahi, K. Wei, A. Tello, E. Armagan, L.F. Boesel, F. Sorin, R. M. Rossi, T. Defraeye, C. Toncelli, Facile Fabrication of Microfluidic Chips for 3D Hydrodynamic Focusing and Wet Spinning of Polymeric Fibers, Polymers 12 (3) (2020) e633.

[49] D. Garlotta, A literature review of poly (lactic acid), J. Polym. Environ. 9 (2001) 63–84, https://doi.org/10.1023/A:1020200822435.

[50] Y. Si, T. Ren, B. Ding, J. Yu, G. Sun, Synthesis of mesoporous magnetic Fe3O4@carbon nanofibers utilizing in situ polymerized polybenzoxazine for water purification, J. Mater. Chem. 22 (11) (2012) 4619–4622, https://doi.org/10.1039/c2jm00036a.

[51] R. Casasola, N.L. Thomas, A. Trybala, S. Georgiadou, Electrospun poly lactic acid (PLA) fibres: Effect of different solvent systems on fibre morphology and diameter,

Polymer. 55 (18) (2014) 4728–4737, https://doi.org/10.1016/j.polymer.2014.06.032.
[52] A.S.D.W.C. National Research Council, Toxicity of Selected Organic Contaminants in Drinking Water, National Academies Press (US)1982.
[53] S. Biswas, S.N. Talapatra, Microbial volatile organic compounds as indoor air pollutants: prediction of acute oral toxicity, hepatotoxicity, immunotoxicity, genetic toxicity endpoints, nuclear receptor signalling and stress response pathways by using protox–II webserver, J Adv. Sci. Res. 10 (03) (2019) 186–195.
[54] J.P. Torré, D. Haillot, S. Rigal, R. de Souza Lima, D. c, b. j.-p.,, 1,3 Dioxolane versus tetrahydrofuran as promoters for CO 2 -hydrate formation: Thermodynamics properties, and kinetics in presence of sodium dodecyl sulfate, Chem. Eng. Sci. 126 (2015) 688–697, https://doi.org/10.1016/j.ces.2015.01.018.
[55] S.E. Morgan, M.L. Willis, G.W. Peterson, J.J. Mahle, G.N. Parsons, Green MOF-Fabrics: Benign, Scalable Sorption-Vapor Synthesis of Catalytic Composites to Protect against Phosphorus-Based Toxins, ACS Sustainable Chem. Eng. 10 (8) (2022) 2699–2707, https://doi.org/10.1021/acssuschemeng.1c07512.
[56] J. van Amsterdam, T. Brunt, E. Pennings, W. van den Brink, Risk assessment of GBL as a substitute for the illicit drug GHB in the Netherlands. A comparison of the risks of GBL versus GHB, Regul. Toxicol. Pharmacol. 70(2) (2014) 507-513. Doi: 10.1016/j.yrtph.2014.08.014.
[57] J.E. Camp, S.B. Nyamini, F.J. Scott, Cyrene is a green alternative to DMSO as a solvent for antibacterial drug discovery against ESKAPE pathogens, RSC Med. Chem. 11 (1) (2020) 111–117, https://doi.org/10.1039/c9md00341j.
[58] Y. Matsuda, A. Fukatsu, Y. Wang, K. Miyamoto, J.W. Mays, S. Tasaka, Fabrication and characterization of poly(l-lactic acid) gels induced by fibrous complex crystallization with solvents, Polymer 55 (16) (2014) 4369–4378, https://doi.org/10.1016/j.polymer.2014.06.086.
[59] P. Shaiju, N.S. Murthy, E.B. Gowd, Molecular, Crystalline, and Lamellar Length-Scale Changes in the Poly(l-lactide) (PLLA) during Cyclopentanone (CPO) Desorption in PLLA/CPO Cocrystals, Macromolecules 49 (1) (2015) 224–233, https://doi.org/10.1021/acs.macromol.5b02425.
[60] J. Yan, Y. Zheng, Y. Zhou, Y. Liu, H. Tan, Q. Fu, M. Ding, Application of infrared spectroscopy in the multiscale structure characterization of poly(l-lactic acid), Polymer 278 (2023) e125985.
[61] A. Leroy, S. Ribeiro, C. Grossiord, A. Alves, R.H. Vestberg, V. Salles, C. Brunon, K. Gritsch, B. Grosgogeat, Y. Bayon, FTIR microscopy contribution for comprehension of degradation mechanisms in PLA-based implantable medical devices, J. Mater. Sci. Mater. Med. 28(6) (2017) 87 1-13. Doi: 10.1007/s10856-017-5894-7.
[62] L.-R.N. Meaurio E, Sarasua J R. , Infrared spectrum of poly (L-lactide): Application to crystallinity studies, Macromolecules, 39(26) (2006) 9291-9301. Doi: 10.1021/ma061890r.
[63] T. Hongen, T. Taniguchi, S. Nomura, J.-I. Kadokawa, K. Monde, In Depth Study on Solution-State Structure of Poly(lactic acid) by Vibrational Circular Dichroism, Macromolecules 47 (15) (2014) 5313–5319, https://doi.org/10.1021/ma501020s.
[64] N.M. Praveena, P. Shaiju, R.B.A. Raj, E.B. Gowd, Infrared bands to distinguish amorphous, meso and crystalline phases of poly(lactide)s: Crystallization and phase transition pathways of amorphous, meso and co-crystal phases of poly(L-lactide) in the heating process, Polymer 240 (2022) e124495.
[65] Y.-H. Gong, C. Shen, Y.-Z. Lu, H. Meng, C.-X. Li, Viscosity and Density Measurements for Six Binary Mixtures of Water (Methanol or Ethanol) with an Ionic Liquid ([BMIM][DMP] or [EMIM][DMP]) at Atmospheric Pressure in the Temperature Range of (293.15 to 333.15) K, J. Chem. Eng. Data 57 (1) (2011) 33–39, https://doi.org/10.1021/je200600p.
[66] N. Kaerkitcha, S. Chuangchote, K. Hachiya, T. Sagawa, Influence of the viscosity ratio of polyacrylonitrile/poly(methyl methacrylate) solutions on core–shell fibers prepared by coaxial electrospinning, Polym. J. 49 (6) (2017) 497–502, https://doi.org/10.1038/pj.2017.8.
[67] W. Jeong, J. Kim, S. Kim, S. Lee, G. Mensing, D.J. Beebe, Hydrodynamic microfabrication via"on the fly" photopolymerization of microscale fibers and tubes, Lab Chip 4 (6) (2004) 576–580, https://doi.org/10.1039/b411249k.
[68] F. Zarrin, N.J. Dovichi, Sub-picoliter detection with the sheath flow cuvette, Anal. Chem. 57 (13) (1985) 2690–2692, https://doi.org/10.1021/ac00290a057.
[69] Y.Q. Jignesh P S., Kamalesh K. S., Basil C. B., Nanofiltration based diafiltration process for solvent exchange in pharmaceutical manufacturing, J. Membr. Sci. 211 (2) (2003) 251-261. Doi: 10.1016/S0376-7388(02)00423-4.
[70] A. Misefari, Investigation of the spectroscopic, chemical and physical properties of Cyrene and its hydrate, University of York, 2017.
[71] A. Salisu, M.M. Sanagi, A. Abu Naim, K.J. Abd Karim, W.A. Wan Ibrahim, U. Abdulganiyu, Alginate graft polyacrylonitrile beads for the removal of lead from aqueous solutions, Polym. Bull. 73 (2) (2015) 519–537, https://doi.org/10.1007/s00289-015-1504-3.
[72] M. Murariu, A.-L. Dechief, R. Ramy-Ratiarison, Y. Paint, J.-M. Raquez, P. Dubois, Recent advances in production of poly(lactic acid) (PLA) nanocomposites: a versatile method to tune crystallization properties of PLA, Nanocomposites 1 (2) (2014) 71–82, https://doi.org/10.1179/2055033214y.0000000008.
[73] W. Yu, X. Wang, E. Ferraris, J. Zhang, Melt crystallization of PLA/Talc in fused filament fabrication, Mater. Des. 182 (2019) e108013.
[74] Z. Zhu, Y. Bian, X. Zhang, R. Zeng, B. Yang, Study on the crystallization behavior and conformation adjustment scale of poly(lactic acid) in the terahertz frequency range, Phys. Chem. Chem. Phys. 25 (12) (2023) 8472–8481, https://doi.org/10.1039/d3cp00208j.
[75] R. Nirmala, K.T. Nam, R. Navamathavan, S.J. Park, H.Y. Kim, Hydroxyapatite mineralization on the calcium chloride blended polyurethane nanofiber via biomimetic method, Nanoscale Res. Lett. 6 (2011) 1–8, https://doi.org/10.1007/s11671-010-9737-4.
[76] Y. Li, Y. Li, C. Li, X. Zhang, F. Zeng, H. Lin, Z. Su, Optical and mechanical properties of NaCl: Ce3+ crystal grown by the Czochralski method, J. Mater. Sci: Mater. Electron. 31 (16) (2020) 13070–13077, https://doi.org/10.1007/s10854-020-03857-y.
[77] M.L. Di Lorenzo, R. Androsch, Influence of α′-/α-crystal polymorphism on properties of poly(l-lactic acid), Polym. Int. 68 (3) (2019) 320–334, https://doi.org/10.1002/pi.5707.
[78] E.W. Fischer, H.J. Sterzel, G. Wegner, Investigation of the structure of solution grown crystals of lactide copolymers by means of chemical reactions, Colloid Polym. Sci. 251 (1973) 980–990, https://doi.org/10.1007/BF01498927.
[79] B. Gupta, N. Revagade, N. Anjum, B. Atthoff, J. Hilborn, Preparation of poly(lactic acid) fiber by dry–jet–wet spinning. II. Effect of process parameters on fiber properties, J. Appl. Polym. Sci. 101 (6) (2006) 3774–3780, https://doi.org/10.1002/app.23543.
[80] Y.Z. Quan Quan, H. Piao, H. Zhang, J. Zhao, Polybutyrolactam (PBY) fiber: a promising biobased and biodegradable fiber fabricated by dry-jet-wet spinning, Polymer. 260 (2022) e125392.
[81] A.R. Liberski, J.T. Delaney Jr., H. Schafer, J. Perelaer, U.S. Schubert, Organ weaving: woven threads and sheets as a step towards a new strategy for artificial organ development, Macromol. Biosci. 11 (11) (2011) 1491–1498, https://doi.org/10.1002/mabi.201100086.
[82] A. Duval, L. Avérous, Dihydrolevoglucosenone (Cyrene™) as a versatile biobased solvent for lignin fractionation, processing, and chemistry, Green Chem. 24 (1) (2022) 338–349, https://doi.org/10.1039/d1gc03395f.
[83] A. Czapka, C. Grune, P. Schadel, V. Bachmann, K. Scheuer, M. Dirauf, C. Weber, A. L. Skaltsounis, K.D. Jandt, U.S. Schubert, D. Fischer, O. Werz, Drug delivery of 6-bromoindirubin-3'-glycerol-oxime ether employing poly(D, L-lactide-co-glycolide)-based nanoencapsulation techniques with sustainable solvents, J. Nanobiotechnol. 20 (1) (2022) 5, https://doi.org/10.1186/s12951-021-01179-7.